Pázmány Péter Catholic University

Faculty of Information Technology and Bionics

Roska Tamás Doctoral School of Sciences and Technology

Erzsébet Hakkel

Regulation of energy homeostasis by hypothalamic circuits; light- and electron microscopic studies in rodents

Ph.D Dissertation

Thesis Advisor:

Csaba Fekete D.Sc.

Budapest, 2017

"Research is to see what everybody else has seen, and to think what nobody else has thought."

Albert Szent-Györgyi

Abstract

The incidence of obesity increased rapidly in the developed countries during the last decades. Obesity has high impact on the population health and also on the health care cost. Therefore, understanding the regulatory mechanisms of the energy homeostasis has critical importance. The goal of our studies was to better understand the regulation of the energy homeostasis by hypothalamic circuits. The hypothalamic paraventricular nucleus (PVN) is an important hypothalamic centre in the regulation of the energy homeostasis. Using electron microscopy, we demonstrated that the nitric oxide (NO) system is anatomically positioned to be utilized as both anterograde and retrograde transmitter system in the PVN. The association of the NO synthesizing enzyme, the neuronal nitric oxide synthase (nNOS), to the postsynaptic side of synapses formed by type 1 cannabinoid receptor (CB1)-containing axons in the parvocellular part of the PVN suggests that the NO and the endocannabinoid systems may interact in the regulation of presynaptic terminals of parvocellular neurons. Our *in vivo* studies revealed that both the NO and the endocannabinoid systems of the PVN are involved in the regulation of the energy homeostasis by neuropeptide Y (NPY) an orexigenic peptide of the hypothalamic arcuate nucleus (ARC). While inhibition of the NO system inhibits the effects of NPY on the food intake, inhibition of CB1 in the PVN markedly decreases the effect of NPY on the energy expenditure. The hypophysiotropic thyrotropin-releasing hormone (TRH)-synthesizing neurons of the PVN play important role in the regulation of energy expenditure by controlling the hormone synthesis of the thyroid gland. We demonstrated that the axon terminals of these neurons contain the thyroid hormone transporter monocarboxylate transporter 8 (MCT8) in the external zone of the median eminence (ME) where these terminals are closely associated with tanycytes, the cell type that expresses the thyroid hormone activating type 2 deiodinase suggesting that the TRH neurons accumulate the active thyroid hormone, T3, from the ME where T3 originates from the blood and from tanycytes.

The non-hypophysiotropic TRH neurons in the perifornical area/BNST region express a second anorexigenic peptide, the urocortin 3 (UCN3). We showed that these TRH/UCN3 neurons form symmetric type synaptic associations with the anorexigenic POMC neurons of the ARC raising the possibility that the TRH/UCN3 neurons regulate the food intake *via* the POMC neurons of the ARC.

In addition, we demonstrated that TRH-containing axons densely innervate the histaminergic neurons in all subnuclei of the tuberomammillary nucleus indicating that the histaminergic neurons may receive feeding related inputs from non-hypophysiotropic TRH populations.

Acknowledgements

*Firstly, I would like to thank my scientific advisor **Csaba Fekete** for his guidance, patience and valuable support during my studies.*

*I am also grateful to **Balázs Gereben**, **Imre Farkas** and **Zsolt Liposits** for their help in my studies.*

*I thank my former and current colleagues **Anett Szilvásy-Szabó, Andrea Kádár, Ágnes Simon, Andrea Juhász, Anikó Zeöld, Barbara Vida, Csaba Vastagh, Csilla Molnár, Enikő Kiss, Erik Hrabovszky, Flóra Bálint, Györgyi Zséli, Imre Kalló, Judit Szabon, Kata Skrapits, Mónika Tóth, Petra Mohácsik, Vera Maruzs, Zoltán Péterfi, Zsuzsa Beliczai** and **Zsuzsa Bardóczi**.*

*I would also like to acknowledge the very important contribution of the co-authors of our papers **Anna Sárvári, Gábor Wittmann, Kata Nagyunyomi-Sényi, László Barna, Masahiko Watanabe, Motokazu Uchigashima, Miklós Palkovits, Raphaël G. P. Denis, Ronald M. Lechan, Serge Luquet, Tamás Füzesi, Ann Marie Zavacki, Rafael Arrojo e Drigo, Liping Dong, Beáta A. Borsay, László Herczeg, Antonio C. Bianco**.*

*Furthermore, I am thankful to the Doctoral School; especially to **Prof. Péter Szolgay** for the opportunity to participate in the doctoral program. I thank **Katinka Tivadarné Vida** for her always kind help and patience to make the administrative side of life easier.*

*I am very grateful to my mother and my friends who always believed in me and supported me. Finally, I am especially appreciated my husband **András** for all his love, patience, support and encouragement that gave me the strength to go on even in the hardest periods of this journey.*

List of abbreviations

2-AG	– *2-arachidonoylglycerol*
AGRP	– *agouti-related neuropeptide*
ARC	– *arcuate nucleus*
BAT	– *brown adipose tissue*
BBB	– *blood-brain-barrier*
BNST	– *bed nucleus of stria terminalis*
cAMP	– *cyclic adenosine monophosphate*
CART	– *cocaine- and amphetamine-regulated transcript*
CB1	– *type 1 cannabinoid receptor*
CCK	– *cholecystocinin*
CNS	– *central nervous system*
CRFR2	– *corticotropin-releasing factor receptor 2*
CRH	– *corticotropin-releasing hormone*
CSF	– *cerebrospinal fluid*
D2	– *deiodinase 2*
DAB	– *diaminobenzidine*
DAGLα	– *diacylglycerol lipase alpha*
DMN	– *dorsomedial nucleus*
eNOS	– *endothelial nitric oxide synthase*
GABA	– *gamma-aminobutyric acid*
GPCR	– *G-protein-coupled receptor*
H1R	– *histamine 1 receptor*
HDC	– *histidine decarbocylase*
HPA	– *hypothalamus – pituitary – adrenal axis*
HPT	– *hypothalamus – pituitary – thyroid*
iNOS	– *inducible nitric oxide synthase*
IR	– *immunoreactive*
KO	– *knock out*
MAP2	– *microtubule-associated protein 2*
MC3R	– *melanocortin 3 receptor*
MC4R	– *melanocortin 4 receptor*
ME	– *median eminence*
MR	– *Mammillary recess*

mRNA	–	*messenger ribonucleic acid*
MTC8	–	*monocarboxylase 8*
NiDAB	–	*nickel diaminobenzidine*
nNOS	–	*neuronal nitric oxide synthase*
NO	–	*nitric oxide*
NOS	–	*nitric oxide synthase*
NPY	–	*neuropeptide Y*
NTS	–	*nucleus tractus solitary*
OATP1C1	–	*organic anion-transporting polypeptide 1c1*
PB	–	*phosphate buffer solution*
PBS	–	*phosphate buffered saline*
PFA	-	*paraformaldehyde*
PHAL	–	*Phaseolus vulgaris leucoagglutin*
PLCß	–	*phospholipase C beta*
POMC	–	*proopiomelanocortin*
PPII	–	*pyroglutamyl peptidase II*
PVN	–	*paraventricular nucleus*
PYY	–	*peptide YY*
sGC	–	*soluble guanylate cyclase*
SS	–	*somatostatin*
T3	–	*triiodothyronine*
T4	–	*thyroxine*
THß2	–	*thyroid hormone ß2 receptor*
TMN	–	*tuberomammillary nucleus*
TRH	–	*thyrotropin-releasing hormone*
TSH	–	*thyroid-stimulating hormone*
UCN3	–	*urocortin 3*
VGLUT1	–	*vesicular glutamate transporter 1*
VGLUT2	–	*vesicular glutamate transporter 2*
VIAAT	–	*vesicular inhibitory amino acid transporter*
α-FMH	–	*alpha-fluoro-methyl histidine*
α-MSH	–	*alpha melanocyte-stimulating hormone*

Table of Contents

List of figures

List of tables

I.   Introduction

The obesity epidemic is one of the major health problem of our days [1]. More than 60% of the population is overweight or obese in the USA and in Europe [2]. Obesity is not only esthetical problem, but it is also major risk factor of devastating diseases like type 2 diabetes, cardiovascular diseases, cancer *etc…* [1]. Despite the very high impact on population health and healthcare cost, efficient, non-invasive and side effect free treatment is currently not available against obesity. Large pharmaceutical companies try to develop efficient anti-obesity drugs based on the currently available drug targets without major breakthrough indicating the necessity of the discovery of novel anti-obesity drug targets. Therefore, better understanding of the regulatory mechanisms of energy homeostasis has critical importance in the fight against obesity.

I.1   Role of the hypothalamic arcuate nucleus (ARC) in the regulation of the energy homeostasis

Information about the actual conditions of energy stores and about the consumed food is transmitted toward the central nervous system via peripheral nerves like the vagus nerve and the sensory fibers of sympathetic nerves and also by changes of the level of circulating hormones like leptin, ghrelin, cholecystokinin (CCK), peptide YY (PYY) and insulin [3]. This communication is critical for the maintenance of energy homeostasis [3]. Genetic alterations in these pathways cause obesity syndrome like in leptin or leptin receptor deficient animals or humans and in mice lacking insulin receptor in the brain [4-8].

A critical brain area that can sense these energy homeostasis related humoral signals is the ARC [3]. Ablation of the ARC by neonatal monosodium glutamate treatment induces obesity and leptin resistance [9].

At least two major energy homeostasis-related neuronal groups are located in the ARC [3]. There is a ventromedially located orexigenic neuronal population that expresses two potent orexigenic peptides, the neuropeptide Y (NPY) and the agouti-related protein (AGRP) [3]. These neurons also express the classical transmitter gamma-aminobutyric acid (GABA) [10] that has been also shown to stimulate food intake [11]. NPY is one of the most potent orexigenic signals [3]. Central administration of NPY causes marked increase of food intake, weight gain and increased adiposity [12]. The effect of NPY on the weight gain, however, cannot be exclusively accounted to its effect on the food intake. NPY also has potent inhibitory effect on the energy expenditure [13]. NPY elicits these effect *via* the G protein coupled postsynaptic Y1 and Y5 receptors [12].

11

AGRP also increases the food intake and inhibits the energy expenditure [14]. The effect of AGRP on the energy homeostasis is mediated by two centrally expressed melanocortin receptors, the melanocortin 3 and 4 receptors (MC3R and MC4R). AGRP is the endogenous antagonist of these receptors [14]. Changes of energy availability regulate the expression of both peptides in the ARC neurons. While fasting stimulates the NPY and AGRP expression in these neurons, leptin administration inhibits the synthesis of the orexigenic peptides [3]. However, genetic ablation of NPY or AGRP has no major effect on the energy homeostasis; the critical importance of the orexigenic ARC neurons has been demonstrated by the life threatening anorexia of mice after ablation of the NPY/AGRP neurons [15, 16].

The proopiomelanocortin (POMC) and cocaine- and amphetamine-regulated transcript-(CART) synthesizing neurons located in the lateral part of the ARC has opposite effect on the regulation of energy homeostasis [3]. The POMC derived α-melanocyte-stimulating hormone (α-MSH) is well known about its potent anorexigenic effect [3]. Central administration of α-MSH reduces food intake and simultaneously increases the energy expenditure [3]. The α-MSH exerts its effect as the agonist of the MC3R and MC4R [17]. CART also inhibits food intake and can completely block the NPY induced feeding response [18]. Currently, little information is available about the effect of CART on the energy expenditure. The receptor(s) of CART has not been identified yet.

The POMC/CART neurons are sensitive to the effects of peripheral energy homeostasis-related hormones, like leptin and insulin [3], but these neurons are regulated differently than the NPY/AGRP neurons. Fasting inhibits the POMC and CART synthesis, while leptin administration stimulates the expression of these genes [3]. Despite the presence of leptin receptor in these cells, indirect effect of leptin that is mediated by GABAergic neurons is also critical in the regulation of the POMC/CART neurons [19].

The importance of the POMC/CART neurons in the regulation of energy homeostasis was also demonstrated by genetic studies. Genetic ablation of the POMC or MC4R genes results in morbid obesity in mice [20, 21]. Mutations of the melanocortin pathway also cause obesity in humans. Indeed, mutations of this pathway are the most frequent reason of the human monogenic obesity syndromes [22]. The absence of CART has less profound effect [23]. The CART knock out mice develop only late onset obesity [23]. In humans, a single nucleotide polymorphism (A1475G) of the CART gene is associated with human obesity syndrome [23].

The two feeding related neuronal populations of the ARC sense and integrate the energy homeostasis related signals and transmit it toward the so-called second order feeding related neuronal populations, including the hypothalamic paraventricular nucleus (PVN), the

hypothalamic dorsomedial nucleus (DMN) and the histaminergic neurons of the tuberomammillary nucleus (TMN).

In addition to, the homeostatic regulation of the energy homeostasis, the feeding related neurons of the ARC are also involved in the regulation of food intake by adverse conditions like infection and stress [24, 25].

I.2 Role of the PVN in the regulation of energy homeostasis

The PVN is a triangular shaped nucleus that is located on the two sides of the upper part of the third ventricle. It consists of magnocellular and parvocellular parts [26]. The oxytocin- and vasopressin-synthesizing neurons of the magnocellular part are involved in the regulation of the posterior pituitary function [26].

The parvocellular part can be further divided into five subdivisions: the anterior, periventricular, medial, ventral and lateral subdivisions and the dorsal cap [27]. The periventricular, and medial parvocellular subdivisions house both hypophysiotropic and non-hypophysiotropic neurons, while the other parvocellular subdivisions house only non-hypophysiotropic neurons.

The hypophysiotropic neurons project to the external zone of the median eminence where they secrete their hypophysiotropic hormones into the extracellular space around the fenestrated capillaries [26]. These hormones reach the anterior pituitary *via* the hypophyseal portal circulation and regulate the hormone production of this endocrine gland. There are three types of hypophysiotropic neurons in the parvocellular part of the PVN: the somatostatin-, the corticotropin-releasing hormone- (CRH) and the thyrotropin-releasing hormone- (TRH) synthesizing neurons. The somatostatin neurons inhibit the growth hormone synthesis of the pituitary, while the hypophysiotropic CRH and TRH neurons are the central regulators of the hypothalamic-pituitary-adrenal (HPA) and thyroid (HPT) axes, respectively. All of these neuroendocrine axes have major impact on the regulation of the energy homeostasis.

A large population of the non-hypophysiotropic neurons in the parvocellular part of the PVN regulates autonomic functions. These neurons project to the intermediolateral column of the spinal cord and to brainstem nuclei involved in the regulation of energy homeostasis like the nucleus tractus solitarii (NTS), the dorsal motor nucleus of vagus, the parabrachial nucleus and the catecholaminergic neurons of the ventral medulla [28]. *Via* these nuclei, the PVN multisynaptically linked to the pancreas, white and brown adipose tissue (BAT), liver and muscle [29-31]. Thus, these so-called preautonomic neurons of the PVN can regulate the energy homeostasis by controlling the lipid metabolism and storage, thermogenesis, gluconeogenesis and insulin synthesis [30].

However, the PVN receives energy homeostasis related inputs *via* multiple neuronal pathways and also *via* hormones, one of its most important energy homeostasis related input originates from the ARC [3]. Both the orexigenic and the anorexigenic neuronal groups densely innervate the neurons of the parvocellular part of the PVN [3]. In many instances, the same parvocellular neurons are innervated by both the orexigenic and anorexigenic ARC neurons [27].

The PVN is a critical mediator of the effects of ARC neurons on the energy homeostasis [3]. Focal administration of NPY into the PVN markedly increases food intake [13], increases the carbohydrate utilization [32], decreases the energy expenditure and the uncoupling protein 1 expression in the BAT [33, 34] and induces body weight gain [35].

Both postsynaptic NPY receptors, the Y1 and Y5, are expressed in the PVN [36], coupled to pertussis-toxin sensitive Gi/o proteins [37], and lead to the inhibition of cyclic adenosine monophosphate (cAMP) accumulation by inhibiting adenylate cyclase [38]. Some of the effects of NPY on energy expenditure are exerted through the regulation of TRH and CRH gene expression in the PVN *via* the modulation of the cAMP pathway [39-42]. NPY also has been shown to inhibit the GABAergic inputs of the parvocellular neurons of the PVN [43].

Similarly to NPY, intraPVN administration of AGRP also increases the food intake [44].

In contrast to the orexigenic peptides, α-MSH has potent anorexigenic effect when injected into the PVN [45]. Most of the effects of the α-MSH are mediated by the MC4R. The MC4R knockout (KO) mice are hyperphagic and have decreased energy expenditure [21]. Re-expression of MC4R exclusively in the PVN rescues the hyperphagic phenotype of the MC4R KO mice, but has only little effect on the energy expenditure [46] substantiating the importance of the PVN in the mediation of the effect of melanocortins on the food intake. α-MSH also regulates the HPA and HPT axes by stimulating the CRH and TRH gene expression in the PVN [47, 48].

I.3   Retrograde transmitter systems in the parvocellular part of the PVN

Using patch clamp electrophysiology, our laboratory showed that NPY inhibits both the GABAergic and the glutamatergic inputs of the parvocellular neurons [49]. These effects were completely prevented by the intracellular administration of the calcium chelator drug BAPTA[1] demonstrating that NPY inhibits the inputs of the parvocellular neurons by stimulating retrograde transmitter release of the target cells. [49]. The most widely utilized retrograde transmitter system in the brain is the endocannabinoid system [50]. In the central nervous system (CNS), the primary receptor of the endocannabinoid signaling system is the type 1

---

[1] *1,2-bis(o-aminophenoxy)ethane-N,N,N',N'-tetraacetic acid*

cannabinoid receptor (CB1) [50]. The two most abundant endogenous ligands of this receptor are the 2-arachidonoylglycerol (2-AG) and the anandamide [50]. 2-AG is synthesized by postsynaptic neurons in the perisynaptic region and acts on the CB1 located in the perisynaptic region of the presynaptic terminals [50]. Activation of the CB1 inhibits the activity of the presynaptic terminals [50]. An important regulator of the endocannabinoid synthesis is the synaptic activity. The synthesizing enzyme of 2-AG, the diacylglycerol lipase α (DAGLα), is activated in response to increased synaptic activity which effect is mediated by metabotropic receptors coupled to phospholipase C beta (PLCβ) like metabotropic glutamate receptor 1 and 5, muscarinic acetylcholine (mACh) receptor M1 and M3 [51].

Our laboratory has shown that CB1 is present in both the inhibitory and excitatory terminals innervating the parvocellular neurons in the PVN [52] and the endocannabinoid system has been shown to mediate the effects of ghrelin and the glucocorticoids on the parvocellular neurons of the PVN [53, 54].

We have found that inhibition of CB1 by AM251[2] prevents the effect of NPY on the GABAergic input of parvocellular neurons [49]. However, the dose of AM251 that were sufficient to prevent the effect of ghrelin on the glutamatergic inputs of the parvocellular neurons [53], did not prevent the effects of NPY on the glutamatergic inputs [49] suggesting that other retrograde signaling system(s) is also involved in the mediation of the NPY induced effects (**Fig. 1**).

Nitric oxide (NO) is a gaseous transmitter [55]. NO is synthesized by a family of the NO synthesizing (NOS) enzymes: the neuronal NOS (nNOS), the inducible NOS (iNOS) and the endothelial NOS (eNOS) [55]. Among these enzymes, the nNOS is present in neurons [55]. The most sensitive receptor of NO is the soluble guanylate cyclase (sGC) [55]. In the hippocampus, both the nNOS and the sGC can be observed in both pre- and postsynaptic localization [56] suggesting that NO can serve as both anterograde and retrograde transmitter. Electrophysiological experiments also provided evidence supporting the retrograde transmitter role of NO and the interaction of the endocannabinoid and NO signaling in the presynaptic plasticity in the hippocampal formation [57].

However, nNOS is also present in the PVN, little is known about the localization of the elements of NO signaling in this nucleus and it is also unknown whether NO is utilized as a retrograde transmitter in this nucleus [58].

---

[2] *biarylpyrazole cannabinoid receptor antagonist*
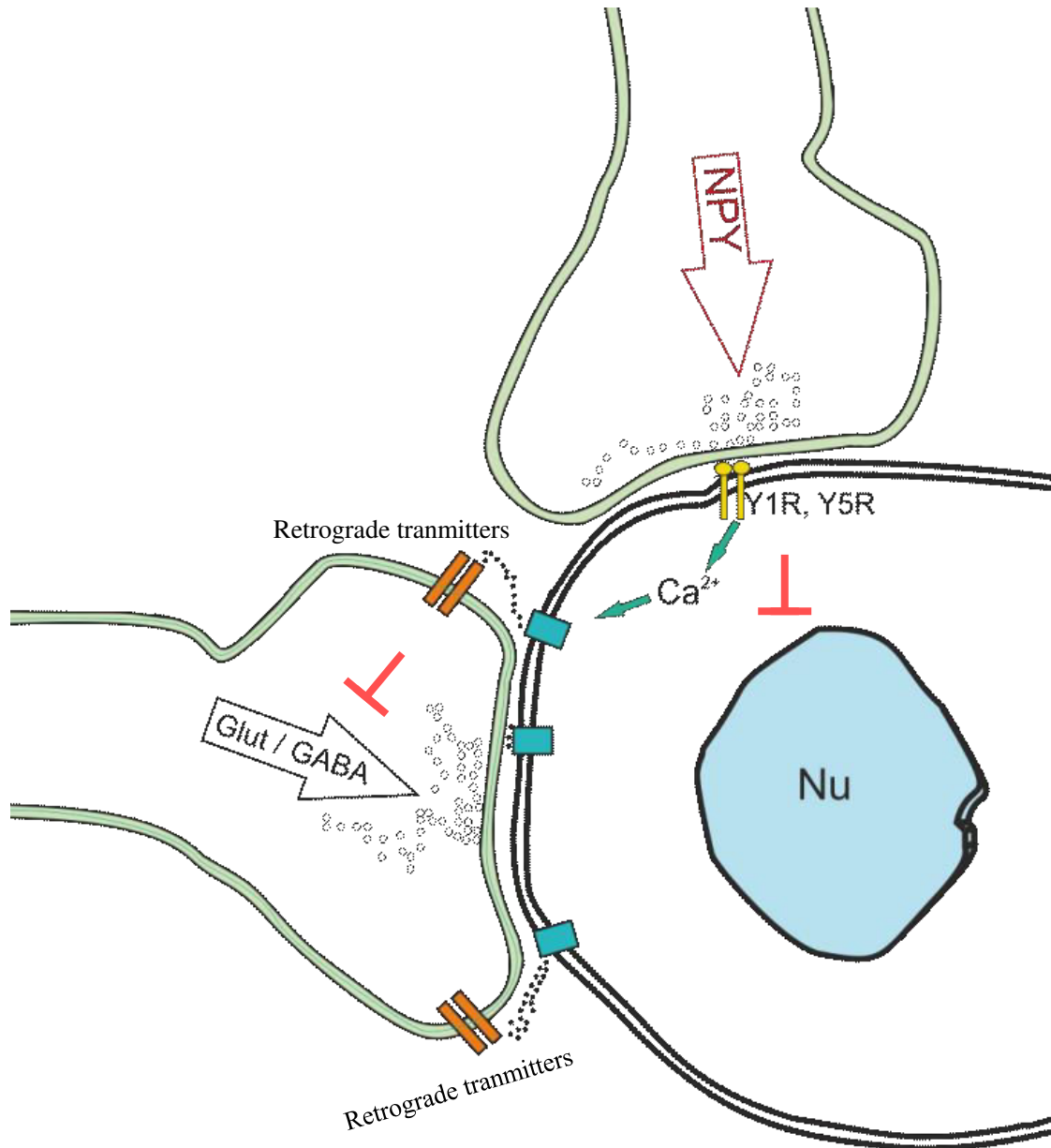
Figure 1 *Schematic illustration of the effect of NPY on the parvocellular neurons in the hypothalamic PVN.*

NPY acts via the Y1 and Y5 receptors in the parvocellular part of the hypothalamic PVN. The receptor activation inhibits gene transcription y decreasing the cAMP level, but at the same time, it can activate retrograde messengers systems via modulation of the intracellular Ca^{2+} levels. Thus, NPY can inhibit the synaptic inputs of the parvocellular neurons via retrograde messengers. Nu –nucleus, Glut – glutamatergic terminals, GABA – GABAergic terminals, NPY-neuropeptide Y, Y1R-NPY receptor type 1, Y5R- NPY receptor type 5

I.4   Feedback regulation of the hypophysiotropic TRH neurons

One of the neuronal groups of the PVN that play critical role in the regulation of the energy homeostasis is the group of the hypophysiotropic TRH neurons [27]. These neurons control the hormone production of the thyroid gland through the regulation of the TSH secretion of

the thyrotroph cells in the anterior pituitary [27]. The thyroid hormones are important regulators of the energy homeostasis [27]. In the absence of thyroid hormones, the basal metabolic rate is decreased by 30% and the cold induced thermogenesis is also absent in hypothyroid animals [27].

The main regulator of the HPT axis is the negative feedback effect of thyroid hormones that ensure the relatively stable circulating thyroid hormone levels [27]. Thus, when the peripheral levels of thyroid hormones are increased, the TRH synthesis is inhibited by thyroid hormones [27]. The hypophysiotropic TRH neurons contain the thyroid hormone β2 receptor (TRß2) that is essential for the feedback regulation of these cells [27]. In addition, implantation of T3[3] adjacent to the PVN inhibits the TRH expression on the side of the implantation [27]. However, restoration of the circulating T3 levels in hypothyroid animals without administration of the prohormone T4[4] is not sufficient to normalize the TRH expression in the PVN [27]. These data demonstrate that hypothalamic conversion of the prohormone T4 to its active form, T3, is necessary for the feedback regulation of the TRH neurons. In the hypothalamus, T4-T3 conversion is catalyzed by the type 2 deiodinase enzyme (D2) [59]. D2 activity or mRNA, however, is not present in the PVN where the hypophysiotropic TRH neurons reside [60]. D2 is synthesized in the hypothalamus by a special glial cell types, the tanycytes [60]. Tanycytes line the lateral wall and the floor of the third ventricle behind the optic chiasm. The long basal process of these cells projects to the hypothalamic dorsomedial and ventromedial nuclei, into the ARC and into the external zone of the median eminence (ME) [27]. Thus, the cell bodies of the TRH neurons are located relatively far from the thyroid hormone activating cells of the hypothalamus. In the external zone of the ME, however, end feet processes of the tanycytes and the axon terminals of the hypophysiotropic TRH neurons are closely associated raising the possibility that T3 released from the tanycytes may be taken up by the hypophysiotropic terminals and transported to the cell bodies of TRH neurons where T3 could bind to the nuclear TRβ2 [27]. The thyroid hormone transport is mediated by thyroid hormone transporters [27]. The main thyroid hormone transporters are the monocarboxylate transporter 8 (MCT8), organic anion-transporting polypeptide 1c1 (OATP1C1), Lat1 and Lat2[5][61]. The main thyroid hormone transporter of neurons is MCT8. The absence of MCT8 causes serious neurological symptom in humans and upregulation of the HPT axis in both humans and mice [62, 63] suggesting that MCT8 is involved in the feedback regulation of the HPT axis. However, the presence of MCT8 was demonstrated in tanycytes [64], data were not available about the presence of this transporter in hypophysiotropic axons. The presence of

---

[3] *triiodothyronine*

[4] *thyroxine*

[5] *heterodimeric large amino acid transporter 1 and 2*

MCT8 in the axon terminals of the hypophysiotropic TRH neurons would suggest that the axon terminals of the hypophysiotropic TRH axons are able to take up T3 in the ME. The importance of this question is underlined by the different kinetics of the T4 and T3 transport through the blood brain barrier (BBB). T3 can far more efficiently pass through the BBB than T4 [27]. This is however not the case in the external zone of the ME which brain region is located outside of the BBB. Thus, the site of thyroid hormone uptake determines whether the hypophysiotropic TRH neurons can only sense the T3 that is activated within the BBB or these cells can sense a mixture of the T3 originating from the circulation and released by the tanycytes in the ME (**Fig. 2**).
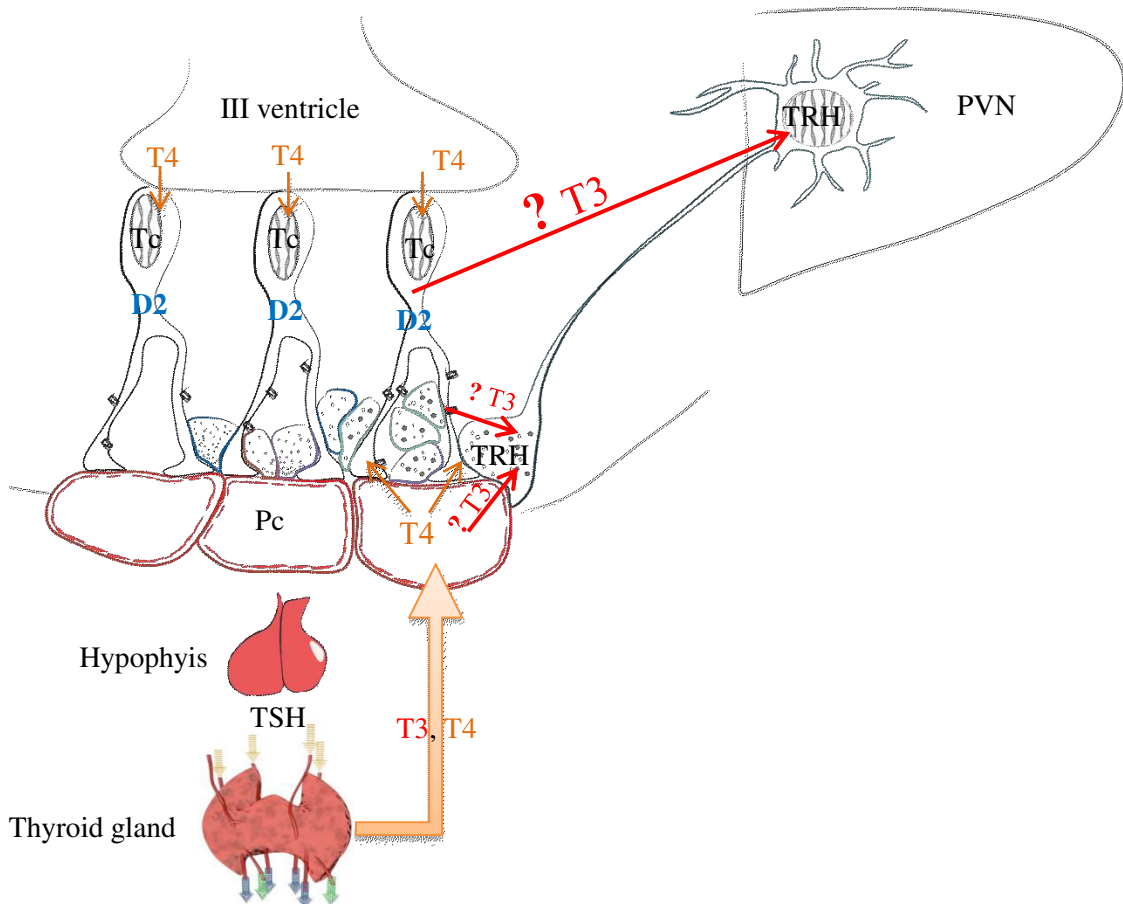
Figure 2 *Schematic illustration of thyroid hormone negative feedback mechanism*

Thyroid hormones exert negative feedback effect on the hypophysiotropic TRH neurons. This feedback mechanism requires central thyroid hormone activation. This T4 to T3 conversion is catalyzed by the type 2 deiodinase (D2) that is expressed by the tanycytes lining the wall of the third ventricle. It was not clear, how T3 released from tanycytes can reach the hypophysiotropic TRH neurons in the PVN. T3 may diffuse through the neuropil. An alternative hypothesis is that the axons of TRH neurons may take up the T3 in the external zone of the median eminence where the axons of hypophysiotropic TRH neurons and the endfeet processes of tanyctes are closely associated D2- type 2 deiodinase enzyme, ME –

18

median eminence, PVN – paraventricular nucleus, TRH – thyrotropin-releasing-hormone, MCT8 – monocarboxylate transporter 8, T3 – triiodothyronine, T4 – thyroxine, TSH – thyroid-stimulating hormone, Pc – portal capillary

I.5 Role of TRH neurons in the regulation of food intake

It was demonstrated decades ago that central administration of TRH decreases food intake and the time spent with feeding [65]. TRH can inhibit even the vigorous feeding when food is reintroduced after a period of fasting [65]. Despite the very robust anorexigenic effect of TRH, very little information is available which TRH cell population and where exerts this effect.

In addition to the very well-known hypophysiotropic TRH neurons in the medial and periventricular parvocellular subdivisions of the PVN, there are many non-hypophysiotropic TRH synthesizing neuronal groups in the brain including the TRH neurons in the anterior and lateral parvocellular parts and dorsal cap of the PVN and TRH neurons in the DMN, lateral hypothalamus, perifornical region, bed nucleus of stria terminalis (BNST) [66].

Our laboratory has shown [67] that a seemingly continuous population of TRH neurons in the perifornical region and BNST area expresses a second anorexigenic peptide, the urocortin 3 (UCN3) and demonstrated that these neurons project to the lateral part of the ARC. The presence of two anorexigenic peptides in the same neurons and the projection of these cells to the lateral part of the ARC where the anorexigenic POMC neurons are located raised the possibility that the TRH/UCN3 neurons of the perifornical area/BNST region could be involved in the regulation of food intake.

Another cell population that may be involved in the mediation of the anorexigenic effects of TRH is the histaminergic neurons of the TMN in the posterior hypothalamus. Similarly to TRH, central administration of histamine reduces food intake in a number of experimental models [68-70]. Furthermore, the absence of the histamine-synthesizing enzyme, the histidine decarboxylase (HDC), results in late onset obesity and hyperphagia [71] demonstrating the anorexigenic role of histamine.

Central administration of TRH not only decreases food intake in a dose-dependent manner, but also increases the concentration of histamine and t-methylhistamine (a major metabolite of neuronal histamine) in the TMN [72] suggesting that the histaminergic neurons may be involved in the mediation of TRH induced anorexia. This hypothesis is further supported by the data that the anorexic effects of TRH could be attenuated by pretreatment with the irreversible HDC inhibitor, α-fluoro-methyl histidine [72] and that TRH can excite the histaminergic neurons [73]. Based on these important functional data, we hypothesized that the identification of the sources of the TRH-containing inputs of the histaminergic neurons can be used to identify anorexigenic TRH cell populations. However, it was unknown, whether

TRH neurons innervate the histaminergic neurons and whether TRH neurons innervate the histaminergic neurons in all five subnuclei of the TMN or the communication of these two systems is localized to only certain TMN subnuclei. Therefore, the detailed description of the relationship of the TRH axons and the histaminergic neurons was necessary to provide anatomical data for later track tracing studies.

II.   Specific aims

To better understand the hypothalamic network regulating energy homeostasis we:

1. Elucidated the ultrastructural localization of the elements of the NO transmitter system in the PVN.

2. Studied whether the NO and the endocannabinoid systems are associated to the same synapses of the parvocellular neurons of the PVN.

3. Examined the role of the endocannabinoid and the NO systems of the PVN in the mediation of the NPY induced regulation of energy homeostasis

4. Determined the presence of MCT8 thyroid hormone transmitter in the axon terminals of the hypophysiotropic TRH neurons.

5. Examined the role of TRH/UCN3 neurons of the perifornical area/BNST region in the regulation of the feeding related neuronal groups of the hypothalamic arcuate nucleus.

6. Studied the TRH-containing innervation of the histaminergic neurons in TMN.

III. Materials and methods

III.1 Animals

The experiments were carried on adult, male Wistar rats (Charles Rivers, Wilmington, MA), CD1 mice (Charles Rivers, Wilmington, MA) and MCT8 KO [74] mice housed under standard environmental conditions (light between 06:00 and 18:00 h, temperature 22±1 °C, rat chow and water *ad libitum*). The used animals are listed in the description of each experiment. All experimental protocols were reviewed and approved by the Animal Welfare Committee at the Institute of Experimental Medicine of the Hungarian Academy of Sciences.

III.2 Colchicine treatment

As peptides are rapidly transported into axons, immunocytochemistry can detect the axons of peptide producing neurons, but can only visualize the perikarya of only a small proportion of these cells. The visualization of peptide synthesizing perikarya can be facilitated by the central administration of the microtubules association inhibitor colchicine, which treatment prevents the axonal transport [75]. Therefore, colchicine-treatment of rats was performed in studies IV.3 and IV.4. Rats anaesthetized with a mixture of ketamine and xylazine (ketamine 50 mg/kg, xylazine 10 mg/kg body weight, ip.) were injected intracerebroventricularly with 100 µg colchicine in 5 µl 0.9% saline under stereotaxic control to facilitate the visualization of peptides in perikarya in the ARC and TMN. Twenty hours later, the animals were anaesthetized and perfused with fixative.

III.3 Fixation of animals for immunocytochemistry at light and electron microscopic levels

Under general anaesthesia (ketamine 50 mg/kg, xylazine 10 mg/kg body weight, ip.), the animals were perfused transcardially by 10 ml phosphate buffer saline (PBS) pH 7.5 followed by fixative solution. The different fixatives used in the studies are summarized in **Table 1**. For light microscopic studies, we used 4% PFA (pH 7.4) to perfuse the animals. This fixative is appropriate for light microscopic studies, and compatible for most antibodies, but it does not provide sufficient tissue preservation for ultrastructural studies. Three of the used antibodies, the sheep and mouse anti-TRH sera and the sheep anti-histamine serum require acrolein-containing fixative that is appropriate for both light- and electron microscopic studies. The rabbit anti-nNOS and the rabbit anti-sGCα sera were not compatible with strong fixatives like acrolein and glutaraldehyde that are routinely used for ultrastructural studies. Therefore, double pH fixatives were used for ultrastructural studies with these antibodies. First the animals were perfused with 4% PFA in sodium-acetate buffer pH 6.0, followed by 4% PFA in

borate buffer pH 8.5. This combination provides good ultrastructure and was compatible with these two antisera. After perfusion, the brains were rapidly removed and stored in 4% paraformaldehyde (PFA) in 0.1M phosphate buffer (PB), pH 7.4 for 2 h for light microscopy or 24 h for electron microscopy. The different antibodies used in the studies are summarized in **Table 2-4**.

Table 1 *Summary of the fixation methods and the number of used animals*

Experiments	Fixative solution	Used amount of the fixative solution	Number of used animals
IV.1.1- 2. Ultrastructural localization of nNOS, sGCα1 and CB1	10 ml of 4% PFA in Na-acetate buffer, pH 6.0, followed by 50 ml of 4% PFA in Borax buffer, pH 8.5	50 ml/mouse	4
IV.1.3. Double-, triple- and quadruple-labeling light microscopic immunocytochemistry using MAP2, VGLUT1, VGLUT2, VIAAT, CB1 and DAGLα antibodies	4% PFA in 0.1 M PB, pH 7.4	50 ml/mouse	3
IV. 2. 1. Light microscopic detection of MCT8	4% PFA in 0.1 M PB, pH 7.4	50 ml/mouse or 150 ml/rat	3 3
IV.2.2. Ultrastructural detection of MCT8	2% PFA + 4% acrolein in 0.1 M PB, pH 7.4	150 ml/rat	3
IV.3. Double- and triple-labeling light- and double-labeling electron microscopic examination of the TRH and UCN3-IR innervation of the α-MSH-IR neurons	3% PFA + 1 % acrolein in 0.1 M PB, pH 7.4	150 ml/rat	3
IV.4. Double-labeling light- and electron microscopic examination of the TRH-IR innervation of the histaminergic neurons	2% PFA + 4% acrolein in 0.1 M PB, pH 7.4	150 ml/rat	3

III.4   Tissue preparation for light microscopic immunohistochemistry

The brains were cryoprotected in 30% sucrose in PBS at 4 °C overnight, then frozen in powdered dry ice. Serial, 25 μm thick coronal sections were cut on a freezing microtome

(Leica, Wetzlar, Germany), collected in cryoprotectant solution (30% ethylene glycol; 25% glycerol; 0.05 M phosphate buffer (PB) and stored at −20 °C until use. The free aldehyde groups in acrolein fixed tissues can bind antibodies, therefore these aldehyde groups can cause high background signal [76]. To prevent this effect, acrolein fixed tissues were treated with 1% sodium borohydride in distilled water (DW) for 30 min. All tissues were treated with 0.5% Triton X-100/0.5% H_2O_2 in PBS for 15 min to increase antibody penetration and reduce endogenous peroxidase activity. To limit the nonspecific antibody binding, the sections were treated with 2% normal horse serum (NHS) in PBS for 20 min.

Table 2 *Summary of the primary and secondary antibodies used in light microscopic studies*

Study number	Used primary antibodies and sources	Dilution	Secondary antibody
IV.2.	rabbit anti-MCT8 (kind gift from Dr. TJ Visser Rotterdam, The Netherlands)	1:5000 – 10000	biotinylated donkey anti-rabbit IgG, 1:500; Jackson ImmunoResearch
IV.4.	sheep anti-TRH (#08W2) [67, 77]	1:50000	biotinylated donkey anti-sheep IgG, 1:500; Jackson ImmunoResearch
	sheep anti-histamine [78]	1:1000	biotinylated donkey anti-sheep IgG, 1:500; Jackson ImmunoResearch

III.5 Tissue preparation for ultrastructural studies

After the perfusion with fixative, the brains were rapidly removed and postfixed in 4% PFA in 0.1M PB, pH 7.4 and overnight at 4°C. Serial, 25-50 μm thick, coronal sections were cut on a Leica VT 1000S vibratome (Leica Microsystems, Wetzlar, Germany) and collected in PBS. Those sections which were fixed with acrolein containing fixative were treated with 1% sodium borohydride in 0.1 M PB, pH 7.4, for 30 min. All sections were treated by 0.5% H_2O_2 in PBS for 15 min. The sections were cryoprotected in 15% sucrose in PBS for 15 min at room temperature (RT) and in 30% sucrose in PBS overnight at 4 °C. The sections were placed in a tinfoil dish or an Eppendorf tube and quickly frozen over liquid nitrogen, then thawed at RT. This cycle was repeated three times to improve antibody penetration into the tissue. To reduce the nonspecific antibody binding, the sections were treated with 2% NHS in PBS for 20 min.

Table 3 *Summary of the primary and secondary antibodies used in fluorescence microscopic studies*

Study number	Used primary antibodies and sources	Dilution	Secondary antibody
IV. 1.2.	rabbit anti-CB1 serum (Abcam, Cambridge UK) [79]	1 µg/ml	Alexa 488-conjugated donkey anti-rabbit IgG, 1:200; Life Technologies
	rabbit anti- DAGLα serum (Abcam, Cambridge UK) [80]	1 µg/ml	Alexa 647-conjugated donkey anti-rabbit IgG, 1:200; Life Technologies
	mouse anti-MAP2 antibody (Millipore)	1 µg/ml	Alexa 405-conjugated donkey anti-mouse IgG, 1:200; Life Technologies
	guinea pig anti-nNOS serum (Abcam, Cambridge UK) [81]	1 µg/ml	Alexa 555-conjugated donkey anti-guinea pig IgG, 1:200; Life Technologies
	goat anti-VGLUT1 serum (Abcam, Cambridge UK) [82]	1 µg/ml	Alexa 555-conjugated donkey anti-goat IgG, 1:200; Life Technologies
	goat anti-VGLUT2 serum (Abcam, Cambridge UK) [82]	1 µg/ml	Alexa 555-conjugated donkey anti-goat IgG, 1:200; Life Technologies
	goat anti-VIAAT serum (Abcam, Cambridge UK) [82]	1 µg/ml	Alexa 555-conjugated donkey anti-goat IgG, 1:200; Life Technologies
IV.2.	rabbit anti-MCT8 serum kind (gift from Dr. TJ Visser Rotterdam, The Netherlands)	1:1000	Alexa 555-conjugated donkey anti-goat IgG, 1:500; Life Technologies
	sheep anti-TRH serum #08W2 [67]	1:1500	Fluorescein DTAF-conjugated donkey anti - sheep IgG, 1:50;Jackson ImmunoResearch
IV.3	rabbit anti-UCN3 serum (kind gift from Dr. WW.Vale La Jolla, CA) [67]	1:60000	biotinylated donkey anti-rabbit IgG, at 1:500; Jackson ImmunoResearch Fluorescein DTAF-conjugated Streptavidin 1:300; Jackson ImmunoResearch
	mouse anti-TRH serum [83, 84]	1:4000	Alexa 555-conjugated donkey anti-mouse IgG, 1:500; Jackson ImmunoResearch
	sheep anti-α-MSH serum	1:20000	Cy5-conjugated donkey anti-sheep IgG, 1:100; Jackson ImmunoResearch
	sheep anti-NPY serum (kind gift from I. Merchenthaler, Baltimore MD)	1:8000	Cy5-conjugated donkey anti-sheep IgG, 1:100; Jackson ImmunoResearch
IV.4.	mouse anti-TRH serum	1:4000	Alexa 555-conjugated donkey anti-mouse IgG, 1:500; Jackson ImmunoResearch
	sheep anti-histamine serum	1:20000	donkey biotinylated anti-sheep IgG, 1:500 fluorescein-conjugated streptavidin, 1:250; Vector Laboratories

Table 4 *Summary of the primary and secondary antibodies used in electron microscopic studies*

Studies number	Used primary antibody and sources	Dilution	Secondary antibody
IV.1.1.	rabbit anti-nNOS serum (Zymed Laboratories, Waltham, MA)	1:200	donkey anti-rabbit IgG-conjugated with 0.8 nm colloidal gold, 1:100; Electron Microscopy Sciences
IV.1.1.	rabbit anti-sGCα1 serum (Sigma Aldrich St. Louis, MA)	1:4000	biotinylated donkey anti-rabbit IgG, 1:500; Jackson Immunoresearch
IV.1.3.	rabbit anti-nNOS serum (Zymed Laboratories, Waltham, MA)	1:200	donkey anti-rabbit IgG-conjugated with 0.8 nm colloidal gold, 1:100; Electron Microscopy Sciences
	sheep anti-CB1 serum (kind gift from Dr. Watanabe, Sapporo, Japan)	1:800	biotinylated donkey anti-sheep IgG, 1:500; Jackson ImmunoResearch
IV.2.	rabbit anti-MCT8 serum (kind gift from Dr. TJ Visser, Rotterdam, The Netherlands)	1:20000	biotinylated donkey anti-rabbit IgG, 1:500; Jackson ImmunoResearch
IV.3.	sheep anti-α-MSH serum (kind gift from Dr. JB Tatro, Boston, MA)	1:1000	donkey anti-sheep IgG-conjugated with 0.8 nm colloidal gold, 1:100; Electron Microscopy Sciences
	rabbit anti-UCN3 serum (kind gift from Dr. WW. Vale, La Jolla, CA)	1:1000	biotinylated donkey anti-rabbit IgG, 1:500; Jackson ImmunoResearch
IV.4.	mouse anti-TRH serum	1:10000	biotinylated donkey anti-mouse IgG, 1:500; Jackson ImmunoResearch
	sheep anti- histamine serum	1:2000	donkey anti-sheep IgG-conjugated with 0.8 nm colloidal gold, 1:100; Electron Microscopy Sciences

III.6   Immunocytochemistry for ultrastructural localization of nNOS

Sections pretreated as described in III.5 were incubated in rabbit anti-nNOS serum (1:200, Zymed Laboratories, Waltham, MA) for 4 days at 4 °C. After rinsing in PBS and in 0.1% cold water fish gelatin (Aurion, Wageningen, Netherlands) /1% bovine serum albumin (BSA) in PBS, the sections were incubated in donkey anti-rabbit IgG-conjugated with 0.8 nm colloidal gold (Electron Microscopy Sciences, Fort Washington, PA) diluted at 1:100 in PBS containing 0.1% cold water fish gelatin and 1% BSA for 1 h. After washing, the sections were fixed in 1.25% glutaraldehyde (Electron Microscopy Sciences, Fort Washington, PA) in 0.1M PB for 10 min. The gold particles were silver intensified with the Aurion R-Gent SE-LM Kit (Aurion, Wageningen, The Netherlands) after rinsing in 0.2M sodium citrate, pH 7.5.

III.7   Immunocytochemistry for ultrastructural localization of sGCα1

Sections pretreated as described in III.5 were placed in rabbit anti-sGCα1 serum (1:4000, Sigma Aldrich, St. Louis, MO) diluted in serum diluent for 4 days at 4 °C. After rinsing in PBS, the sections were incubated in biotinylated donkey anti-rabbit IgG diluted at 1:500 (Jackson Immunoresearch Lab, West Grove, PA) in serum diluent. After rinsing in PBS, and treated with avidin-biotin-complex (ABC elite; 1:1000 dilution; Vector laboratories, Burlingame, CA), the sGCα1-immunoreactivity was detected with NiDAB developer (0.05% DAB, 0.15% nickel-ammonium-sulfate and 0.005% H_2O_2 in 0.05M Tris buffer pH 7.6). The immunoreaction product was silver-intensified by using Gallyas method [85].

III.8   Double-labeling immunocytochemistry for ultrastructural examination of the distribution of nNOS and CB1

Sections pretreated as described in III.5 were placed in a mixture of rabbit anti-nNOS serum (1:200) and sheep anti-CB1 serum (1:800, kind gift from Dr. Watanabe, Sapporo, Japan) for 4 days at 4°C. After rinsing in PBS and 0.1% cold water fish gelatin/1% BSA in PBS, they were incubated in a cocktail of donkey anti-rabbit IgG-conjugated with 0.8 nm colloidal gold (1:100) diluted at 1:100 and biotinylated donkey anti-sheep IgG (Jackson Immunoresearch Lab, West Grove, PA) diluted at 1:500 in PBS containing 0.1% cold water fish gelatin and 1% BSA. After washing, the sections were fixed in 1.25% glutaraldehyde in 0.1M PB for 10 min. The gold particles were silver intensified with the Aurion R-Gent SE-LM Kit after rinsing in 0.2M sodium citrate, pH 7.5, followed by treatment in ABC (1:1000). The CB1-immunoreactivity was detected with NiDAB developer.

III.9   Quadruple-labeling immunofluorescence of the elements of the endocannabinoid and NO signaling systems and markers of glutamatergic and GABAergic neurons in the PVN

Sections pretreated as described in III.4 were incubated in the mixture of primary antibodies overnight (1 µg/ml), and then in a mixture of fluorochrome-conjugated species-specific secondary antibodies for 2 h at (1:200; Life Technologies; Carlsbad, CA). The following primary antibodies were used: rabbit anti-CB1 (Abcam, Cambridge, UK) [79], rabbit anti-DAGLα (Abcam, Cambridge, UK) [80], mouse anti-MAP2 antibody (Millipore, Billerica, MA), guinea pig anti-nNOS (Abcam, Cambridge, UK) [81], goat anti-VGLUT1 (Abcam, Cambridge, UK) [82], goat anti-VGLUT2 (Abcam, Cambridge, UK) [82] and goat anti-VIAAT (Abcam, Cambridge, UK) [82] antibodies. PBS containing 0.1% Tween20 was used as dilution and as washing buffer.

III.10   Light microscopic detection of MCT8

Sections pretreated as described in III.4 containing the ME, were incubated in rabbit anti-MCT8 serum (rat and WT and MCT8 KO mouse tissues; 1:5000–10000; kind gift of Dr. TJ Visser Rotterdam, The Netherlands) for 2 days at 4°C. The sections were then incubated in biotinylated donkey anti-rabbit IgG (1:500) for 2 hours, followed by incubation in ABC (1:1000) for 1 hour. The peroxidase signal was visualized with a NiDAB developer. The resulted reaction product was silver-gold-intensified using the Gallyas method [86].

III.11   Ultrastructural detection of MCT8-immunoreactivity in the rat ME

To study the cellular and subcellular distribution of MCT8 in the rat ME, sections pretreated as described in III.5 were incubated in the primary antibody (anti-MCT8 antiserum; 1:20000) for 36–48 h at 4°C, followed by biotinylated donkey anti-rabbit IgG (1:500) for 2 h and ABC (1:1000) for 1.5 h. The immunoreactive (IR) sites were visualized with NiDAB developer. Finally the immunoreaction product was silver-gold intensified [86].

III.12   Double labeling immunofluorescence for MCT8 and TRH

Sections pretreated as described in III.4 incubated in rabbit anti-MCT8 serum (1:1000, 48 h), and detected with Alexa 555-conjugated anti-rabbit IgG (1:500, 2 h, Thermo Fisher Scientific, Waltham, MA). Then, the sections were immersed in sheep anti-TRH serum (#08W2, 1:1500) followed by Fluorescein DTAF-conjugated donkey anti sheep IgG (1:50, 2h, Jackson ImmunoResearch, West Grove, PA).

III.13   Triple-labeling immunofluorescence for TRH, UCN3 and α-MSH or NPY

One-in-four series of sections from each brain pretreated as described in III.4 were incubated in rabbit anti-UCN3 serum (kind gift from Dr. WW Vale, La Jolla, CA) at 1:60000 dilution, preabsorbed with 75 µg/ml rat CRF (corticotropin-releasing factor) (Bachem, Bubendorf, Switzerland), mouse anti-TRH serum [84] at 1:4000 and either sheep anti-α-MSH serum (kind gift from Dr. JB Tatro, Boston, MA) [78] at 1:20000 or sheep anti-NPY serum (kind gift from Dr. I. Merchenthaler, Baltimore MD) at 1:8000 for 2 days at 4°C. Then, sections were treated with biotinylated donkey anti-rabbit IgG (1:500) for 2 h, followed by the ABC (1:1000) for 2 h. After washes in PBS, sections were subjected to biotinylated tyramide signal amplification using the tyramide signal amplification (TSA) kit according to the manufacturer's instructions (Life technologies, Carlsbad, CA). After further washes, the sections were incubated in a mixture of Fluorescein DTAF-conjugated Streptavidin (1:300, Jackson ImmunoResearch, West Grove, PA), Alexa 555-conjugated donkey anti-mouse IgG (1:500, Jackson

ImmunoResearch, West Grove, PA) and Cy5-conjugated donkey anti-sheep IgG (1:100, Jackson ImmunoResearch, West Grove, PA) for 2 h.

III.14   Double-labeling immunocytochemistry for ultrastructural examination of the UCN3-IR innervation of the α-MSH neurons in the ARC

Sections pretreated as described in III.5 were placed in a mixture of sheep anti-α-MSH serum (1:1000) and rabbit anti-UCN3 serum (1:1000) preabsorbed with 75 µg/ml rat CRF for 4 days at 4 °C. After rinsing in PBS and in 0.1% cold water fish gelatin/1% BSA in PBS, the sections were incubated in donkey anti-sheep IgG-conjugated with 0.8 nm colloidal gold (Electron Microscopy Sciences, Fort Washington, PA) diluted at 1:100 and biotinylated donkey anti-rabbit IgG diluted at 1:500 in PBS containing 0.1% cold water fish gelatin and 1% BSA. After washing, the sections were fixed in 1.25% glutaraldehyde in 0.1M PB for 10 min at RT. After further rinsing in PBS, the sections were washed in Aurion ECS buffer (1:10, Aurion, Wageningen, The Netherlands) diluted in DW. The gold particles were silver intensified with the Aurion R-Gent SE-LM Kit after rinsing in 0.2M sodium citrate, pH 7.5. After treatment in ABC (1:1000), the UCN3-immunoreactivity was detected with NiDAB developer.

III.15   Double labeling immunocytochemistry for TRH and histamine in the TMN

Coronal sections through the posterior hypothalamus were pretreated as described above in III.4 and then were incubated in sheep TRH antiserum [67, 83] at 1:50000 dilution in PBS containing 2% NHS and 0.2% sodium azide for 2 days at 4 °C. After rinses in PBS, the sections were incubated in biotinylated donkey anti-sheep IgG for 2 h (1:500; Jackson ImmunoResearch, West Grove, PA) followed by treatment in ABC (1:1000) in 0.05M Tris buffer for 1 h at RT. The immunoreaction was developed with NiDAB developer. The chromogen was then further intensified by a silver intensification technique to yield a black precipitate [87] After visualization of TRH, the sections were incubated in sheep antiserum to histamine [78] at 1:1000 dilution in antiserum diluent for 2 days at 4 °C, followed by treatment in biotinylated donkey anti-sheep IgG (1:500) and in ABC (1:1000). The immunolabeling was visualized by DAB developer (0.025% DAB/0.0036% H_2O_2 in 0.05M Tris buffer pH 7.6) to yield a brown reaction product. Using the silver intensified NiDAB and DAB fluorochromes sequentially, two antibodies raised the same species can be used for innervation studies without cross-reaction [78, 88] because the use of low pH gold chloride solution during the silver intensification procedure elutes the antigens from the sections [89] and the black silver precipitate completely fills the profiles and thereby obscures any potential, brown, DAB precipitate. Thus, the TRH-IR fibers were labeled by black, silver-intensified Ni-

DAB, and the histamine-IR neurons were labeled with brown DAB, which chromogens could be easily distinguished in the same section.

III.16 Double-labeling immunofluorescence for TRH and histamine in the TMN

To facilitate the quantification of the TRH-IR innervation of the histaminergic neurons, confocal microscopic analyses of double-labeled immunofluorescent sections was performed. Pretreated sections, as described in III.4, containing the TMN were incubated in a mixture of mouse anti-TRH serum [90] at 1:4000 dilution and sheep anti-histamine serum (1:20000) for 2 days at 4 °C. After washing in PBS, the sections were immersed in a mixture of Alexa 555-conjugated donkey anti-mouse IgG (1:500, Jackson ImmunoResearch, West Grove, PA) and biotinylated donkey anti-sheep IgG (1:500) for 2 h at room temperature. This was followed by treatment in ABC (1:1000) diluted in 0.05M Tris buffer for 1 h at room temperature. The sections were then rinsed in PBS and the immunoreaction product was amplified by TSA kit according to the manufacturer's instructions. After further rinses, the sections were incubated in Fluorescein DTAF-conjugated Streptavidin (1:250) for 1 h.

III.17 Double-labeling immunocytochemistry for ultrastructural examination of the TRH-IR innervation of the histamine-IR neurons in the TMN

Sections pretreated as described in III.5 were incubated in mouse anti-TRH serum (1:10000) for 4 days at 4 °C, followed by biotinylated donkey anti-mouse IgG (1:500) for 20 h at 4 °C and ABC (1:1000) for 1 h at RT. Immunoreactivity was detected with DAB developer. The sections were then placed into sheep anti-histamine serum (1:250) for 2 days at 4 °C and after rinsing in PBS and in 0.1% cold water fish gelatin/1% BSA in PBS, the sections were incubated in donkey anti-sheep IgG-conjugated with 0.8 nm colloidal gold diluted at 1:100 in PBS containing 0.1% cold water fish gelatin and 1% BSA. The sections were washed in the same diluent and PBS, followed by a 10 min treatment in 1.25% glutaraldehyde in PBS. After rinsing in Aurion ECS buffer (1:10), the gold particles were silver intensified with the R-Gent SE-LM kit [91].

Table 5 Summary of the antibodies

Used primary antibody	Source	Reference
goat anti-VGLUT1 serum	*Abcam, Cambdridge, UK*	[82]
goat anti-VGLUT2 serum	*Abcam, Cambdridge, UK*	[82]
goat anti-VIAAT serum	*Life technologies, Waltham, MA*	[82]
guinea pig anti-nNOS serum	*Thermo Fisher, Waltham, MA*	[81]
mouse anti-MAP2 antibody	*Millipore, Billerine, MA*	[92]
mouse anti-TRH serum	*Raised in our laboratory*	[83, 84]
rabbit anti- DAGLα serum	*Abcam, Cambdridge, UK*	[80]
rabbit anti-CB1 serum	*Abcam, Cambdridge, UK*	[79]
rabbit anti-MCT8 serum	*kind gift from Dr. TJ Visser, Rotterdam, The Netherlands*	[93]
rabbit anti-nNOS serum	*Zymed Laboratorie, Waltham, MA*	[56]
rabbit anti-sGCα1 serum	*Sigma Aldrich, St. Louis, MA*	[56]
rabbit anti-UCN3 serum	*kind gift from Dr. WW Vale, La Jolle, CA*	[67]
sheep anti-CB1 serum	*kind gift from Dr. M. Watanabe, Sapporo, Japan*	[77]
sheep anti-histamine serum	*Raised in our laboratory*	[78, 84]
sheep anti-NPY serum	*kind gift from Dr. I. Merchenthaler, Baltimore, MD*	[39, 94, 95]
sheep anti-TRH serum	*Raised in our laboratory, #08W2,*	[67, 77, 83]
sheep anti-α-MSH serum	*kind gift from Dr. JB Tatro, Boston, MA*	[96, 97]

III.18 Image analyzes of light microscopic preparations

The sections were mounted on Superfrost slides (Thermofisher, Waltham, MA). Preparations developed with DAB and/or NiDAB developer were coverslipped with DPX mounting medium (Sigma Aldrich, St. Louis, MO), while the immunofluorescent preparations were mounted with the water-based Vectashield mounting medium (Vector Lab., Burlingame, CA) to prevent the fading of the fluorochromes and to avoid the shrinkage of the tissues.

Light microscopic images were taken using a Zeiss AxioImager M1 microscope equipped with AxioCam MRc5 digital camera (Carl Zeiss Inc., Göttingen, Germany).

Immunofluorescent sections were analyzed using a Radiance 2000 confocal microscope (Bio-Rad Laboratories, Hemel Hempstead, UK) using the following laser excitation lines: 488 nm for FITC, 543 nm for Alexa 555 and dichroic/emission filters, 560 nm/500–530 nm for FITC and 570–590 nm for Alexa 555. The high magnification images were taken using 60x oil lens. These images represent a single optical section (less than 0.8 μm thick). For quantitative analyses, series of optical sections were recorded with 0.6 μm Z steps. All labeled neurons were imaged in every forth section of the ARC or the TMN.

Images were analyzed with Laser Vox (Bio Rad Laboratories, Hemel Hempstead, UK) and with Image pro plus software (Media Cybernetics Inc., Bethesda, MD).

The juxtapositions of immunolabeled axon varicosities and the target neurons were traced through the series of optical sections. A varicosity was considered to be juxtaposed to the target neuron if a visible gap was not seen by the observer between the two immunoreactive structures. The quantitative data of the TRH innervation of the histaminergic neurons was analyzed by one way ANOVA analyses followed by Newman Kuels post hoc test using STATISTICA 9 software (StatSoft Inc., Tulsa, OK) [86]. Data are presented as mean ± SEM.

III.19 Embedding, sectioning and examination of preparations for electron microscopic studies

The sections immunostained for ultrastructural studies were osmicated using 1% osmium tetroxide in 0.1M PB for 30 min, and then treated with 2% uranyl acetate in 70% ethanol for 30 min. Following dehydration in an ascending series of ethanol and propylene oxide, the sections were flat embedded in Durcupan ACM epoxy resin (Sigma-Aldrich, St. Louis, MO) on liquid release agent (Electron Microscopy Sciences, Fort Washington, PA)-coated slides, and polymerized at 56 °C for 2 days. Ultrathin 50–70 nm sections were cut with Leica ultracut UCT ultramicrotome (Leica Microsystems, Wetzlar, Germany), collected onto Formvar-coated, single slot grids (Electron Microscopy Sciences, Fort Washington, PA), and examined with a JEOL electron microscope.

III.20 Specificity of antisera

The specificity of the sheep anti-histamine serum [78], the sheep anti-TRH serum [67], rabbit anti-UCN3 serum [67], sheep anti-NPY serum [94] and sheep anti- α-MSH serum [8] was reported previously. Mouse anti-TRH serum was generated similarly to the sheep anti- TRH serum [67]. Briefly, the immunogenic complex was prepared by mixing 25 mg TRH (Bachem AG, Budendorf, Switzerland), 24 mg BSA (Sigma-Aldrich, St. Louis, MO), and 15 μL acrolein (Sigma-Aldrich, St. Louis, MO) in 4 mL PBS. The mixture was kept at room temperature overnight. The reaction was stopped by the addition of 10 mg sodium borohydride. Finally, the conjugate was dialyzed against PBS. For initial immunization, 250 μg TRH-acrolein-BSA complexes in 100 μL PBS was emulsified with an equal volume of Freund's complete adjuvant (Sigma-Aldrich, St. Louis, MO) and injected subcutaneously. Subsequent boosts with Freund's incomplete adjuvant (Sigma-Aldrich, St. Louis, MO) were administered at 28 day intervals. The animals were decapitated 8 days after the third immunization and the serum was separated by centrifugation. The antiserum was affinity-purified on a column loaded with TRH-coupled CNBr-activated Sepharose 4 Fast Flow gel (Amersham Pharmacia Biotech, Buckinghamshire, UK). Specificity of the antiserum for

immunocytochemistry was tested by preabsorption with TRH (Bachem, Bubendorf, Switzerland) at 80 µg/mL concentration, which resulted in the complete loss of immunostaining. Specificity of the antiserum was further verified by double-labeling of sections with the sheep anti-TRH (#08W2,) serum and the well characterized rabbit anti-TRH no. 31 serum [98] which resulted in a complete colocalization of the two signals in axons as well as in cell bodies in colchicine-treated animals.

To test the specificity of the anti-MCT8 antibody in the examined region, hypothalamic sections of MCT8-KO mice were used as a negative control (the MCT8-KO brain was kindly provided by Dr. H. Heuer, Jena, Germany). MCT8-immunoreactivity was completely absent in the median eminence of the MCT8-KO mice (**Fig. 7D, E**). The employed secondary antibodies were designed for multiple labeling and pre-absorbed by the producer with immunoglobulins of several species, including those in which the current non-corresponding primary antibodies were raised. Omission of any of the primary antisera from the multiple-labeling immunofluorescence did not influence the pattern of the other immunoreaction signals.

III.21 Examination of the role of the endocannabinoid and NO transmitter systems in the mediation of the metabolic effects of NPY evoked in the PVN

III.21.1 Implantation of bilateral guide cannula in the PVN of mice

A bilateral 26-gauge, 0.8 mm C/C stainless steel cannula (Plastics One, Roanoke, VA, USA) was stereotaxically implanted into the PVN under isoflurane anesthesia -0.8 mm posterior to bregma and to a depth of -4.8 mm from the surface of the brain, with bregma and lambda kept in the horizontal plane. The cannula was secured to the skull using dental acrylic cement, and then occluded with a dummy cannula. After a week of [67] recovery and demonstration that no loss of body weight was observed, correct placement of the cannula was verified by administration of NPY (0.25 nM/µl at 0.5 µl/min) using a 33-gauge stainless internal injector cannula. Mice that failed hyperphagic food intake (n=0) were removed from the study.

III.21.2 IntraPVN infusions in mice

Peptides and reagents were dissolved in artificial cerebrospinal fluid (aCSF, prepared according to the instructions of Alzet, Cupertino, CA) and infused intraPVN (0.4 µl on each side) at a rate of 0.5 µl/min. Briefly, the bilateral internal cannula was connected to a polyethylene-50 tubing (Alzet, Cupertino, CA), the tubing connected to a 10 µl Hamilton syringe (Hamilton, Reno, NV) and the syringe was driven by a micro pump (KDS scientific, Holliston, MA). Once the internal injector cannula was in place, the animals were set lose

during the infusion (1 min) and the injector cannula maintained in place for another minute before replacing the animals in their cages.

All animals were placed inside the calorimetric cage (TSE system, Frankfurt, Germany) 48 h before the experiment. Animals were kept under a 12 h light/dark cycle from 7.00 AM and housed in a temperature-controlled environment at 22.5 °C with free access to food and drink. Animals were customized daily to manipulation.

Body mass composition (lean tissue mass, fat mass, free water and total water content) was analyzed using an Echo Medical systems' EchoMRI (Whole Body Composition Analyzers, Houston, USA), according to manufacturer's instructions. Briefly, anesthetized mice were weighed before they were put in a mouse holder and inserted in EchoMRI analyzer. Readings of body composition were given within 3 mins. On the day of the metabolic measurements, at 9.00 AM, appropriate intraPVN injections were performed within 4 mins (handling and injection), and the animals placed back into the calorimetric cage in the presence (*ad libitum*) or absence of food. Food was restored to the food restricted animals 7 h after the intraPVN injections.

III.21.3 Measurement of metabolic parameters

In a first series of study, food of animals was removed 30 min before injection to prevent the confounding effects of the consumed food when the effect of intraPVN injections were investigated on parameters of energy homeostasis such as energy expenditure, estimation of basal metabolism, substrate utilization (RER) and locomotor activity. Reagent injection days were alternated with aCSF injection. (i.e.: day 1: aCSF, day 2: NPY, day 3 and 4: aCSF, day 5: NPY + AM251, day 6 and 7: aCSF, day 8: AM251).

In a second, similar injection paradigm, food intake and spontaneous locomotor following intraPVN injections was investigated. Animals were placed in their cages with free access to regular chow. Food consumption, metabolic parameters and locomotor activities were recorded over 8 hours. Finally, caloric response, energy homeostasis and locomotor activity were investigated in animals subject to intraPVN injections of either aCSF or inhibitor N omega-propyl-L-arginine (NPLA)[6] after an overnight fast. Food being replaced 15 min after the initial intraPVN injection.

Mice were analyzed for whole energy expenditure (EE), oxygen consumption and carbon dioxide production, respiratory exchange rate ($RER = VCO_2/VO_2$, where V is a volume), and locomotor activity using calorimetric cages with bedding, food and water (Labmaster, TSE Systems GmbH, Bad Homburg, Germany). The ratio of gases was determined through an indirect open circuit calorimeter [99, 100]. This system monitors O_2 and CO_2 concentration

---

[6] *selective nNOS inhibitor*

by volume at the inlet ports of a tide cage through which a known flow of air is being ventilated (0.4 L/min), and compared regularly to a reference empty cage. The air sensors were calibrated with O2 and CO2 mixture of known concentrations (Air Liquide S.A., Paris, France). Oxygen consumption, carbon dioxide production and EE were recorded every 10 min for each animal during the entire experiment. Whole energy expenditure was calculated using the Weir equation respiratory gas exchange measurements [101]. Ambulatory movement was recorded using an infrared light beam-based activity monitoring system with online measurement at 100 Hz.

Data analysis was performed using Microsoft Excel using extracted raw value of VO2 consumed, VCO2 production (express in ml/h), and energy expenditure (Kcal/h). Subsequently, each value was normalized to whole lean tissue mass extracted from the EchoMRI analysis.

III.21.4 Estimation of basal metabolism

No practical methods of estimation of the basal metabolism are available presently [102]. However, an estimation of basal metabolism was made on the following basis: the basal metabolic rate was calculated from the first experimental set when the animals did not have access to food to avoid confounding thermic effects of food. Data points of EE were considered to be the best estimation of basal metabolism when spontaneous activity during the previous 30 minutes was less than 1% of the highest daily value.

III.21.5 Statistical analysis of the *in vivo* data

The results are expressed as mean ± SEM. Variance equality was analyzed by F test (Microsoft Excel), and comparisons between groups were carried out using Student's t test or nonparametric Mann-Whitney-Wilcoxon's test (Minitab, Paris, France). When appropriate, analyses of variances were performed followed either by a Bonferroni post hoc test with the appropriate parameters (drugs and time), and their interaction as factor (Minitab, Paris, France) a, b, c and d differed significantly ($P<0.05$). Unless otherwise indicated in the text, a P-value of <0.05 was indicated by * and considered statistically significant. Data in the line figures are expressed as means ± SEM of at least 6 observations. Bar graphs represent means ± SEM obtained from ANOVA. For each phase, values (bars) without the same labels (a, b, c and d) differ significantly.

IV.   Results

IV.1   Presence of the NO system and effect of the NO system on the parvocellular part of the PVN

IV.1.1 Elucidation of the ultrastructural localization of the elements of the NO transmitter system in the PVN.

Our laboratory previously demonstrated the presence of CB1 receptor in both inhibitory and excitatory inputs of parvocellular neurons of the mouse PVN [52]. To determine whether NO also can function as a retrograde transmitter in the parvocellular part of the PVN, ultrastructural studies were performed in the periventricular and medial parvocellular parts of the PVN. The nNOS enzyme, the primary neuronal isoform of the NOS family [55] was observed in neuronal perikarya and dendrites (**Fig. 3A-C**) in addition to presynaptic terminals in the parvocellular part of the PVN (**Fig. 3B-D**). In many instances, silver grains denoting nNOS-immunoreactivity were closely associated with the postsynaptic density of both symmetric (**Fig. 3C, D**) and asymmetric type of synapses (**Fig. 3A, B**). Similarly, the alpha 1 subunit of soluble guanylate cyclase (sGCα1), the primary receptor for NO, was also observed in presynaptic terminals (**Fig. 3E, G**) and postsynaptic (**Fig. 3F, H**) elements of both excitatory and inhibitory synapses (**Fig. 3E-H**). These data demonstrate that NO can function as both anterograde and retrograde transmitter in the parvocellular part of the PVN.

36

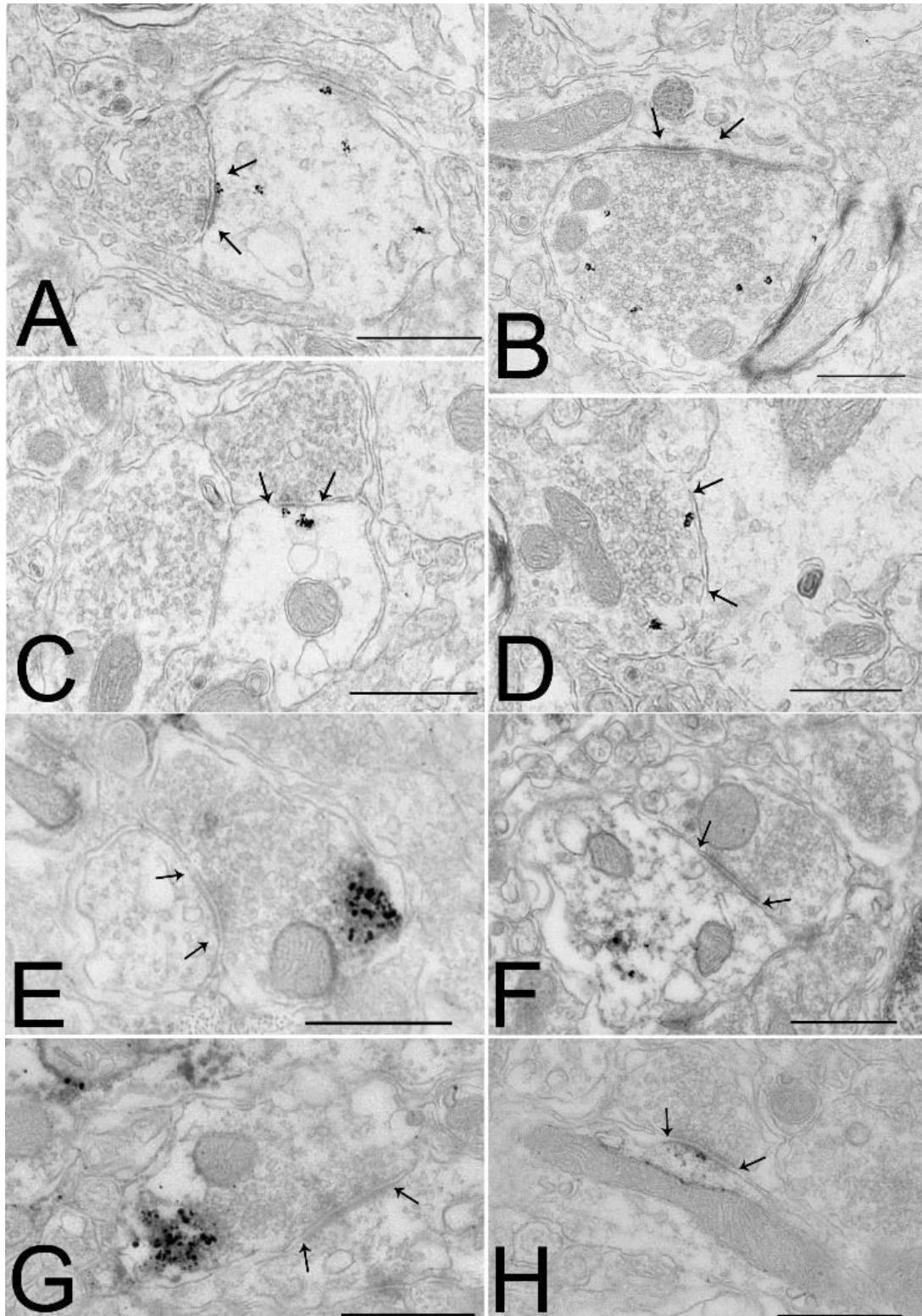***Figure 3*** *Ultrastructural localization of the components of the NO system in the parvocellular part of the PVN in mice.*

*Electron micrographs illustrate the postsynaptic (**A, C**) and presynaptic (**B, D**) localization of nNOS-immunoreactivity in the parvocellular part of the PVN. The nNOS-immunoreactivity is labeled with highly electron dense gold–silver granules and observed in dendrites in the*

*proximity of both asymmetric (**A, B**) and symmetric (**C, D**) synapses. Soluble guanylyl-cyclase alpha 1 subunit-immunoreactivity (sGCα1) is present in presynaptic axons (**E, G**) and dendrites (**F, H**) in the PVN. sGCα1-immunoreactive (sGCα1-IR) is recognized by the presence of the electron dense silver granules in axon varicosities forming both symmetric (**E**) and asymmetric type synapses (**G**). Similarly, sGCα1-IR is seen in the proximity of postsynaptic density of both symmetric (**F**) and asymmetric (**H**) synapses. Arrows point to synapses. Scale bars=0.5µm. a= axon; d= dendrite; Nu= nucleus*

IV.1.2 Anatomical relationship of the endocannabinoid and NO systems in the PVN

To understand whether the endocannabinoid and NO systems regulate the very same neuronal inputs of the parvocellular neurons in the PVN, quadruple-labeling immunocytochemistry was performed using a microtubule-associated protein 2 (MAP2) neuronal marker combined with markers of glutamatergic or GABAergic terminals and components of the endocannabinoid and NO systems. In many instances, nNOS was present in dendrites of parvocellular neurons in the PVN close to the region where CB1-IR glutamatergic (vesicular glutamate transporter 1 and 2 (VGLUT1 and VGLUT2)-IR; **Fig. 4A1,-B2**) or GABAergic (vesicular inhibitory amino acid transporter (VIAAT)-IR; **Fig. 4C1, C2**) terminals form juxtapositions with dendrites. In addition, the endocannabinoid 2-AG synthesizing enzyme, the DAGLα, was observed to colocalize with nNOS in dendrites of parvocellular neurons (**Fig. 4D1-D2**).

To further support the anatomical basis of an interaction between the two retrograde transmitter systems, ultrastructural studies were performed, showing that nNOS is present in close proximity to the postsynaptic site of the synapse of some CB1-IR glutamatergic and GABAergic terminals (**Fig. 4E, F**). These data suggest that the two retrograde transmitter systems may interact in the regulation of the inputs of the parvocellular neurons.
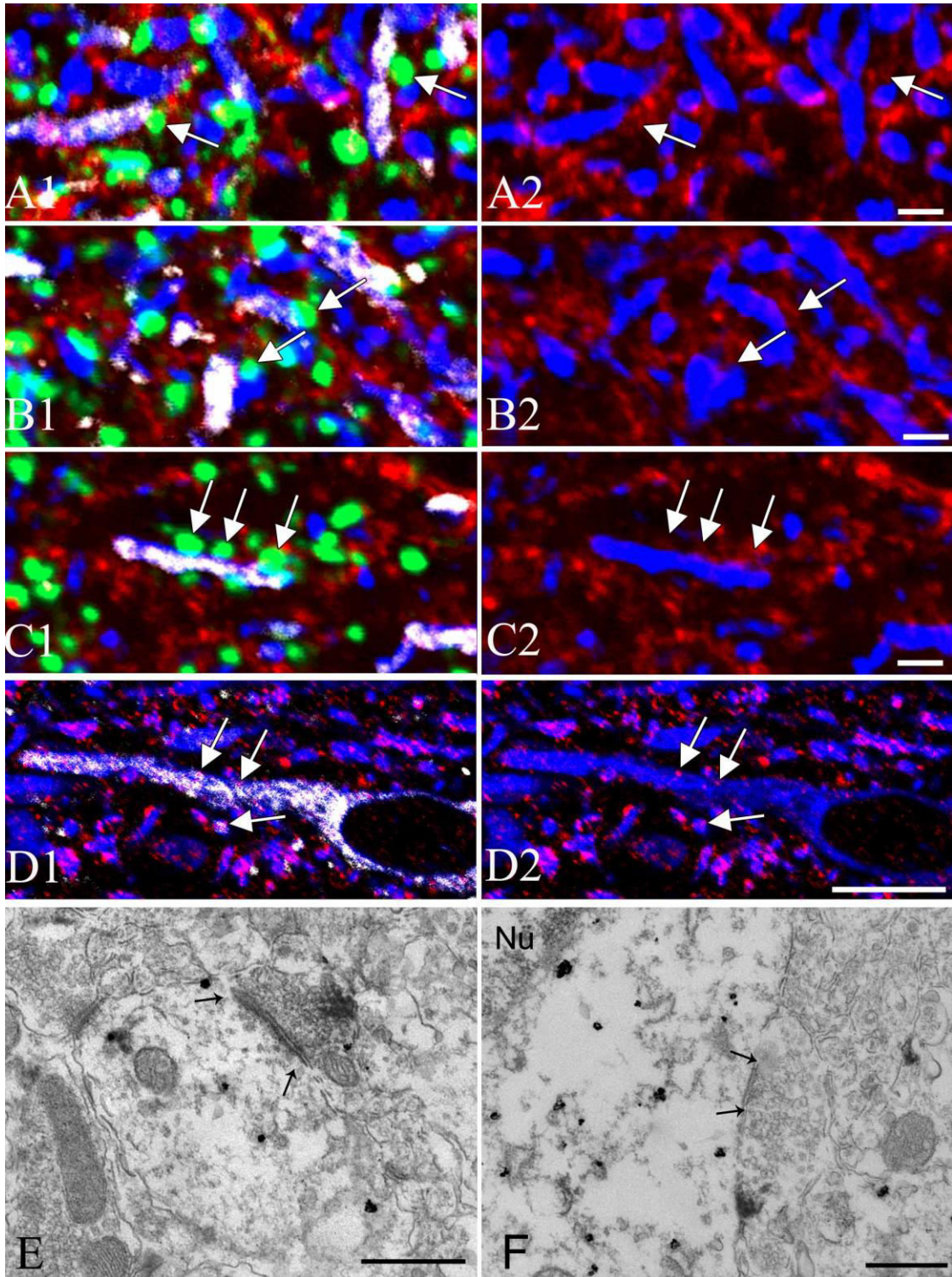
Figure 4 *Association of the endocannabinoid and NO systems with the same synapses of parvocellular neurons in the PVN.*

*Images of quadruple immunolabeling (**A-C**) preparations illustrate the close association of cannabinoid type 1 receptor (**CB1**)- immunoreactive (**IR**) excitatory (**A, B**) and inhibitory (**C**) axon varicosities to neuronal nitric oxide synthase (**nNOS**) containing dendrites in the parvocellular part of the PVN. The axon varicosities of excitatory neurons are labeled with vesicular glutamate transporter 1 (VGLUT1) (**A1**, green) or vesicular glutamate transporter 2*

*(VGLUT2) (**B1**, green)-immunoreactivity, while the inhibitory terminals are labeled with vesicular inhibitory amino acid transporter (VIAAT)-immunoreactivity (**C1**, green). The dendrites are visualized based on their microtubule-associated protein 2 (MAP2)-immunoreactivity (A-C, blue). CB1-immunoreactivity is labeled with red fluorescence, while the nNOS-immunoreactivity is pseudocolored white. For better visualization, the MAP2 and CB1-immunoreactivities in the same field are also shown separately (**A2-C2**). Images of triple-labeled immunofluorescent preparations (**D**) show the colocalization (arrows) of the endocannabinoid synthesizing diacylglycerol lipase alpha (DAGLα) (red) and nNOS (white) in the dendrites (MAP2-IR, blue) of the parvocellular part of the PVN. For better visualization, the MAP2 and CB1-immunoreactivities in the same field are also shown separately (**D2**). Electron micrographs illustrate synaptic associations (arrows) between a nNOS-IR dendrite (**E**) and perikaryon (**F**) with CB1-IR axon terminals. The nNOS-IR elements are labeled with highly electron dense gold–silver granules, while the CB1-IR terminals are recognized by the presence of the electron dense nickel-diaminobenzidine (NiDAB) chromogen. The associations of the two retrograde transmitter systems can be observed in both asymmetric (**E**) and symmetric (**F**) type of synapses in the parvocellular part of the PVN in mice. Arrows point to the synapses. Scale bars = 2μm on (**A-C**), 10μm on (**D**) and 0.5μm on (**E, F**). Nu= nucleus*

IV.1.3 Examination of the role of the endocannabinoid and the NO systems of the PVN in the mediation of the NPY induced regulation of energy homeostasis

To determine the role of the two retrograde transmitter systems in the mediation of the various actions of NPY on the energy balance within the PVN, we studied whether local administration of inhibitors of the endocannabinoid and NO systems influence the effects of NPY on food intake, energy expenditure, substrate utilization and locomotor activity. NPY administration into the PVN (intraPVN) impacted on whole energy expenditure, spontaneous activity and respiratory exchange ratio (RER) with a characteristic biphasic pattern if the animals had no access to food (**Fig. 5F**), in good agreement with previous observations by Ruffin et al [103]. The biphasic response being prototypical of NPY-initiated response, the two phases were independently analyzed. Therefore, the experiments were split into two main periods, 0-2.5h and 2.5-7h, after which food was given to the mice at 7 h.

The first 2.5 h after intraPVN NPY injection was characterized by a slight increase in energy expenditure (P<0.01; **Fig. 5A, B**) primarily assignable to increased locomotor activity (P<0.001; **Fig. 5C, D**). The treatment also increased the carbohydrate utilization evidenced by the increase of RER (P<0.001; **Fig. 5E, F**) compared to aCSF administration. The second phase post injection (2.5h-7h) was characterized by a significant decrease in energy expenditure (**Fig. 5A, B**) and a normalization of both locomotor activity and substrate utilization compared to aCSF treated animals (**Fig. 5C, D, E, F**). These changes persisted until food was reintroduced to the animals at 7h.

Fasting is typically associated with sustained increase in NPY release from ARC neurons to PVN structures and associated with a transient increase in foraging behavior (after an overnight fast) followed by a drastic decrease in activity as a means to conserve energy [104]. A similar change in locomotor activity also occurs in food restricted animals before the time of anticipated feeding when the NPY release is increased in the PVN [105, 106].
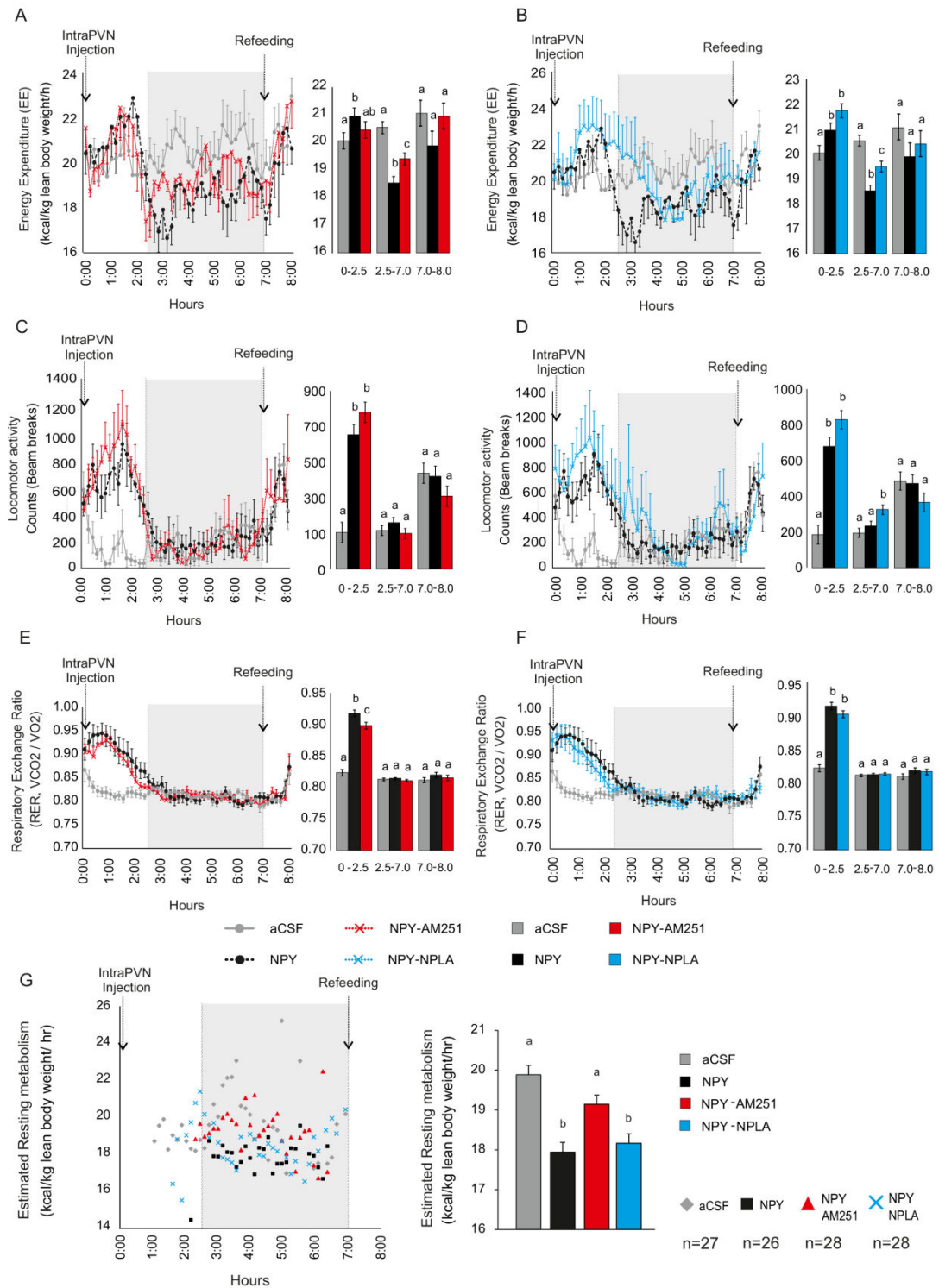
Figure 5 *Effect of intraPVN co-administration of NPY with the CB1 antagonist, AM251, or the nNOS inhibitor, NPLA, on parameters of energy expenditure.*

*Effect of intraPVN co-administration of NPY and AM251 on energy expenditure normalized by total lean body mass (**A**), spontaneous locomotor activity (**C**), and respiratory exchange ratio (RER) (**E**) of n=7-9 mice with no access to food. Effect of intraPVN co-administration of NPY and NPLA on energy expenditure normalized by total lean body mass (**B**), spontaneous locomotor activity (**D**), and respiratory exchange ratio (RER) (**F**) of n=7-9 mice with no*

42

*access to food. Estimation of the resting metabolism of mice injected with NPY alone or co-administrated with AM251 or NPLA (**G**), 27, 26, 28 and 28 points were collected respectively for aCSF, NPY, NPY-AM251 and NPY-NPLA treated groups within the second phase (between 2.5 h and 7 h, grey area). Each group was injected either with aCSF (grey), NPY (black), NPY+AM251 (red), NPY+NPLA (blue) at T=0, and food was replaced at T=7 h. Bar graphs were calculated from the ANOVA analysis for each phase. Data with different superscript letters are significantly different (P<0.05) according to the ANOVA analysis followed by a Bonferroni post hoc test. Data are expressed as mean ± SEM.*

Intra PVN NPY administration seems to recapitulate these behavior outputs in the presence or absence of food (**Fig. 6**).

Local administration of the selective nNOS NPLA resulted in an extended period of increase in locomotor activity (**Fig. 5D**). Antagonizing CB1 signaling pathway through local AM251 administration did not oppose NPY action on locomotor activity, neither in the first nor in the second period (**Fig. 5C**), but resulted in a significant change in substrate utilization as shown by attenuation of the NPY-induced increase in RER during the first, hyperactive period (**Fig. 5E**). NPLA administration, however, did not affect RER in either period (**Fig. 5F**).

Importantly, between 2.5h and 7h, both AM251 and NPLA treatments partially reversed the decrease in energy expenditure induced by NPY (**Fig. 5A, B**). However, the action of NPLA on the NPY-mediated inhibition of energy expenditure could be attributed to the extended hyperactivity (**Fig. 5B**). In contrast, the effect of AM251 on the energy expenditure was not associated with change in locomotor activity (**Fig. 5C**), suggesting that resting energy expenditure might account for this effect. Therefore, resting energy expenditure was calculated during the 2.5-7h period, showing that while AM251 markedly attenuated the inhibitory effect of NPY on resting energy expenditure, NPLA treatment had no effect on this parameter (**Fig. 5G**).

In a separate set of experiments, the involvement of the two retrograde signaling pathways in the mediation of the acute NPY-mediated food intake was investigated. IntraPVN NPY administration resulted in a more than 5-fold increase in food intake and 2-fold increase in locomotor activity during the first 2.5 hours (**Fig. 6B**). Although intraPVN administration of the endocannabinoid antagonist, AM251, alone, or in combination with NPY had a marginal effect on food intake and locomotor activity (**Fig. 6B**), the inhibition of nNOS signaling within the PVN completely prevented the NPY-induced increase in food intake and locomotor activity (**Fig. 6A, B**), while administration of NPLA, alone, had no effect (**Fig. 6C**).

As exogenously administered NPY increased the NPY concentration in the PVN before food was provided in our experimental paradigm, and fasted animals also have increased NPY concentration in the PVN before they receive food, we tested whether inhibition of NO

signaling within the PVN can influence the behavior of fasted and refed mice. IntraPVN administration of nNOS markedly decreased the food intake   in animals refed after fasting, indicating that the endogenously released NPY also utilizes NO to influence this parameter of energy homeostasis (**Fig. 6C**).
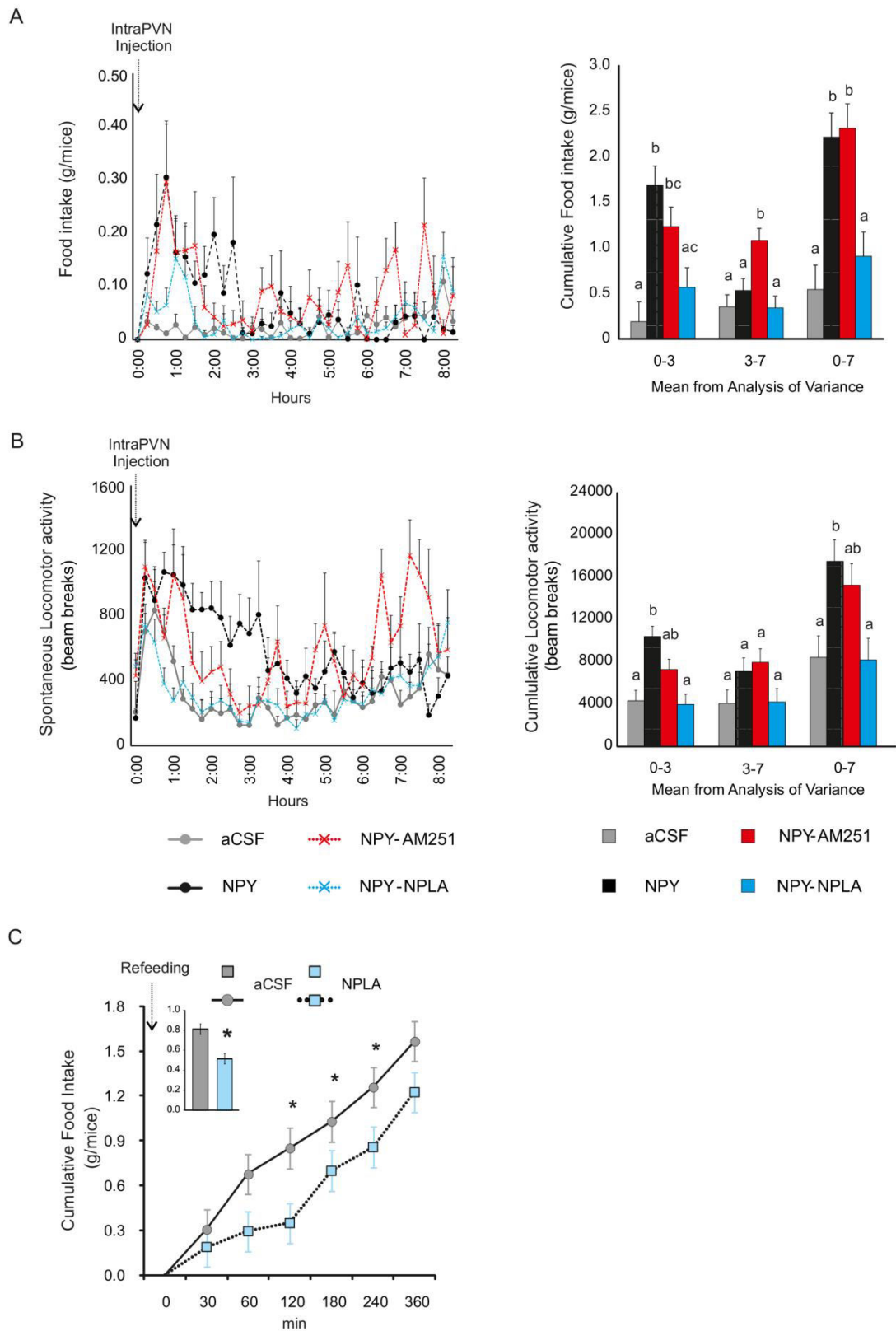
Figure 6 *Food intake (A) and spontaneous activity (B) of mice injected intraPVN with aCSF (grey), NPY (black) alone, co-administrated with AM251 (red) or NPLA (blue).*

*Food intake and spontaneous locomotor activity was monitored over 8 hours post injection. IntraPVN injection of NPLA (light blue) diminished food intake following an overnight fast (**C**). Mean ± SEM extracted from the analysis of variance of food intake and spontaneous locomotor activity are represented in the bar graphs. Data with different superscripts letters are significantly different (P<0.05) according to the ANOVA followed by Bonferroni post hoc test. Data are expressed as mean ± SEM. n = minimum 6 mice per group.*

IV.2 Identification of the presence of MCT8 thyroid hormone transmitter in the axon terminals of the hypophysiotropic TRH neurons.

In the ME, intense and diffuse MCT8-immunoreactivity was observed in cell bodies and processes exhibiting the characteristic distribution and morphology of tanycytes (**Fig. 7A, B**). In addition, punctate MCT8-immunoreactivity was detected among the tanycyte processes in the external zone of the ME (**Fig. 7C**). The specificity of the immunostaining was demonstrated by the absence of immunostaining in MCT8 KO mice (**Fig. 7D, E**). Ultrastructural analysis of the MCT8-IR elements in the external zone of the ME demonstrated strong MCT8-immunoreactivity distributed uniformly in the tanycyte processes (**Fig. 8A**). In addition, MCT8-immunoreactivity was also observed in axon terminals, where the silver grains focally accumulated in a segment of the axon varicosities in close proximity to the plasma membrane (**Fig. 8B, C**).

Double-labeling immunofluorescent staining for MCT8 and TRH demonstrated the presence of MCT8-immunoreactive puncta on the surface of the vast majority of TRH-containing axon varicosities in the external zone of the ME (**Fig. 9**)

47
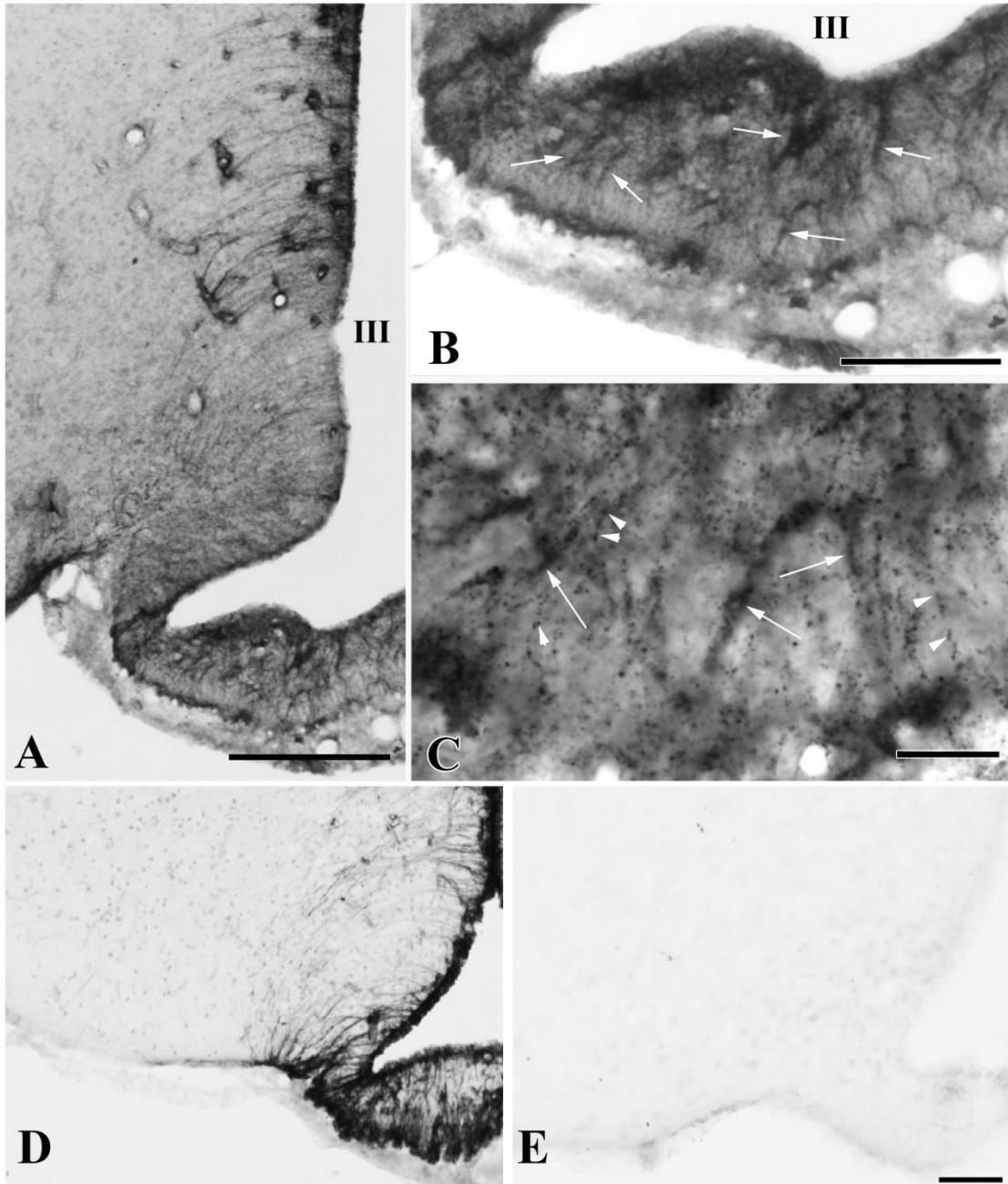
Figure 7 *MCT8 immunoreactivity in the rodent mediobasal hypothalamus.*

*Low magnification photograph illustrates the presence of monocarboxylate transporter 8 (MCT8)-immunoreactivity associated with tanycytes (**A**). In the ME, strong MCT8-immunoreactivity is observed in tanycyte processes (**B, arrows**). In addition to occurring in tanycyte processes (arrows), MCT8-immunoreactivity is also observed in small dot like structures reminiscent of axon varicosities (arrow heads) (**C**). MCT8 immunoreactivity in the mediobasal hypothalamus of wild-type (**D**) and MCT8-KO mice (**E**). III, third ventricle; Scale bars: 200 μm in **A**, 100 μm in **B**, 20 μm in **C**, 50 μm in **D, E**.*
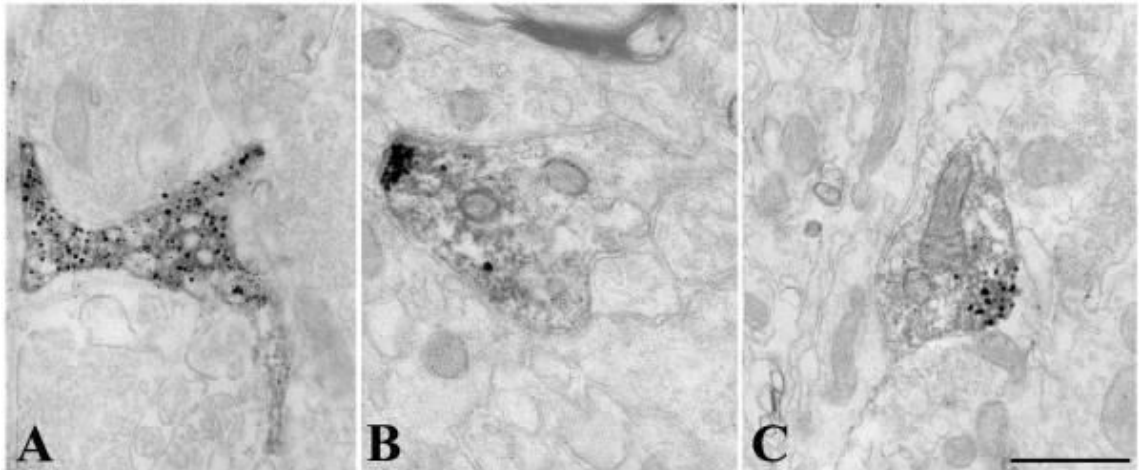
Figure 8 *Ultrastructure of MCT8 immunoreactive structures in the rat ME.*

Monocarboxylate transporter 8 (MCT8)-immunoreactivity (silver grains) is associated with tanycyte (A) and axon varicosities (B, C) in the external zone of the median eminence (ME). In the axon varicosities, silver grains accumulate in a small region of the varicosity close to the cytoplasmic membrane (B, C). Scale bar: 500 nM.
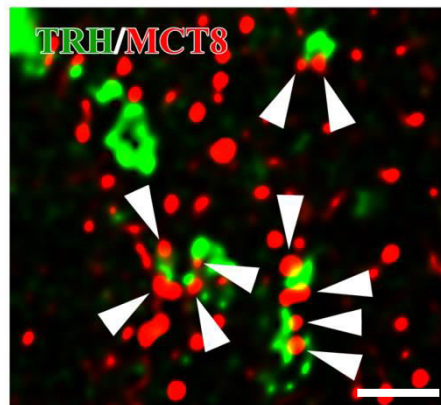
Figure 9 *MCT8 immunoreactivity in axon varicosities of the rat hypophysiotropic TRH neurons.*

The immunofluorescent signal for monocarboxylate transporter 8 (MCT8) (red) is distributed as small dots throughout the external zone of median eminence and appears (arrowheads) on the surface of thyrotropin-releasing hormone (TRH) immunofluorescent axon varicosities (green). Scale bar: 2 μm

IV.3   TRH/UCN3 neurons of the perifornical area/BNST region innervate the POMC neurons of the ARC

Since our laboratory has demonstrated that the vast majority of the neurons co-synthesizing TRH and UCN3 are located in continuous neuronal group located in the perifornical area and in the BNST [67], the colocalization of TRH and UCN3 was used as a marker of axons originating from the TRH/UCN3 neurons of the perifornical area/BNST region. Within the ARC, UCN3-IR axons were primarily observed in the lateral part of the nucleus, while a dense network of TRH-IR axons was observed throughout the entire ARC. The vast majority of UCN3–IR axons contained TRH-immunoreactivity in this nucleus. However, a large portion of TRH-IR axons did not contain UCN3. Double-labeled TRH/UCN3 axons were primarily located in the lateral part of the ARC (**Fig. 10**).

NPY-IR neurons were predominantly localized in the ventromedial part of the ARC where only scattered TRH/UCN3 axons were found (**Fig. 11**). TRH/UCN3-IR axon terminals were observed in juxtaposition to only 4.3±1.3% of NPY-IR neurons. An average of 1.7±0.2 TRH/UCN3 axon varicosities were observed on the surface of the contacted NPY neurons.

The localization of the α-MSH-containing neurons in the ARC, however, overlapped with the distribution of the double-labeled TRH/UCN3-IR axons in the lateral ARC (**Fig. 12A, C, E**). More than a half (52.38±8.5%) of the α-MSH-containing neurons was contacted by TRH/UCN3-IR axon terminals. The average number of TRH/UCN3 axon varicosities was 6.48±0.82 on the contacted α-MSH neuron.

Since the vast majority (88.1±1.2%) of UCN3-IR axon varicosities on the surface of α-MSH-IR neurons also co-contained TRH-immunoreactivity, UCN3-immunoreactivity was used for ultrastructural studies to label the UCN3 axons of perifornical area/BNST region origin.

UCN3-IR axon terminals labeled with nickel-intensified diaminobenzidine (NiDAB) formed synaptic contacts with the silver-intensified immunogold-labeled α-MSH-IR perikarya and dendrites (**Fig. 12G, H**). All observed synapses between these two systems were the asymmetric type.
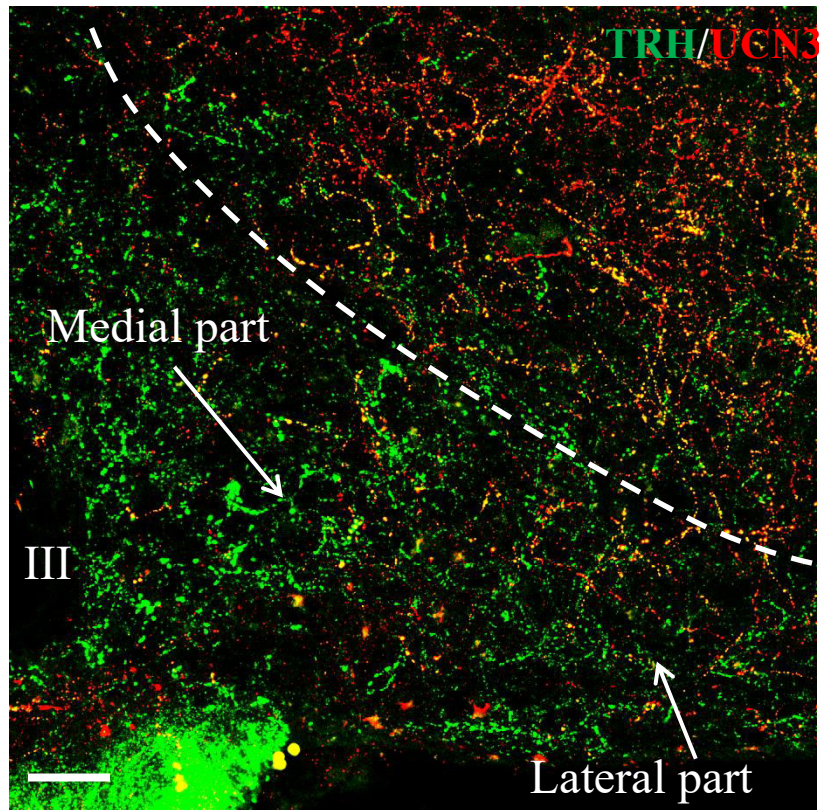
Figure 10 *UCN3-IR (green) and TRH-IR (red) innervation of the ARC in the rat.*

Thyrotropin-releasing hormone (TRH) - immunoreactive (IR) axons densely innervate the entire arcuate nucleus (ARC), while double-labeled.Urocortin3 (UCN3)/TRH axons are concentrated in the lateral part of the nucleus, while only scattered double-labeled axons reside in the medial part of the ARC. III, third ventricle, Scale bar: 50 µM
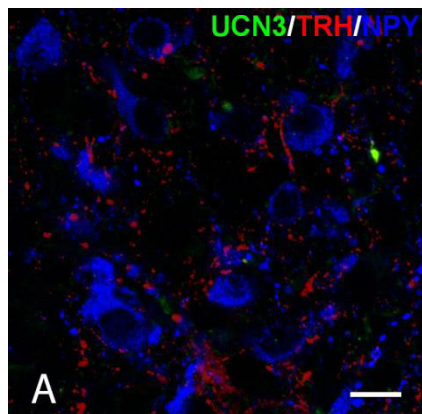
Figure 11 *Relationship of TRH/UCN3- containing axons on the NPY neurons in the ARC.*

Triple-labeled immunofluorescent detection of the urocortin 3 (UCN3) - (green), thyrotropin-releasing-hormone-immunoreactive (TRH-IR) (red) axons and neuropeptide Y (NPY) - (blue) neurons in the arcuate nucleus (ARC). Only scattered double-labeled axons can be observed around the NPY neurons in ventromedial part of the ARC. Scale bar on (**A**) = 10 µm
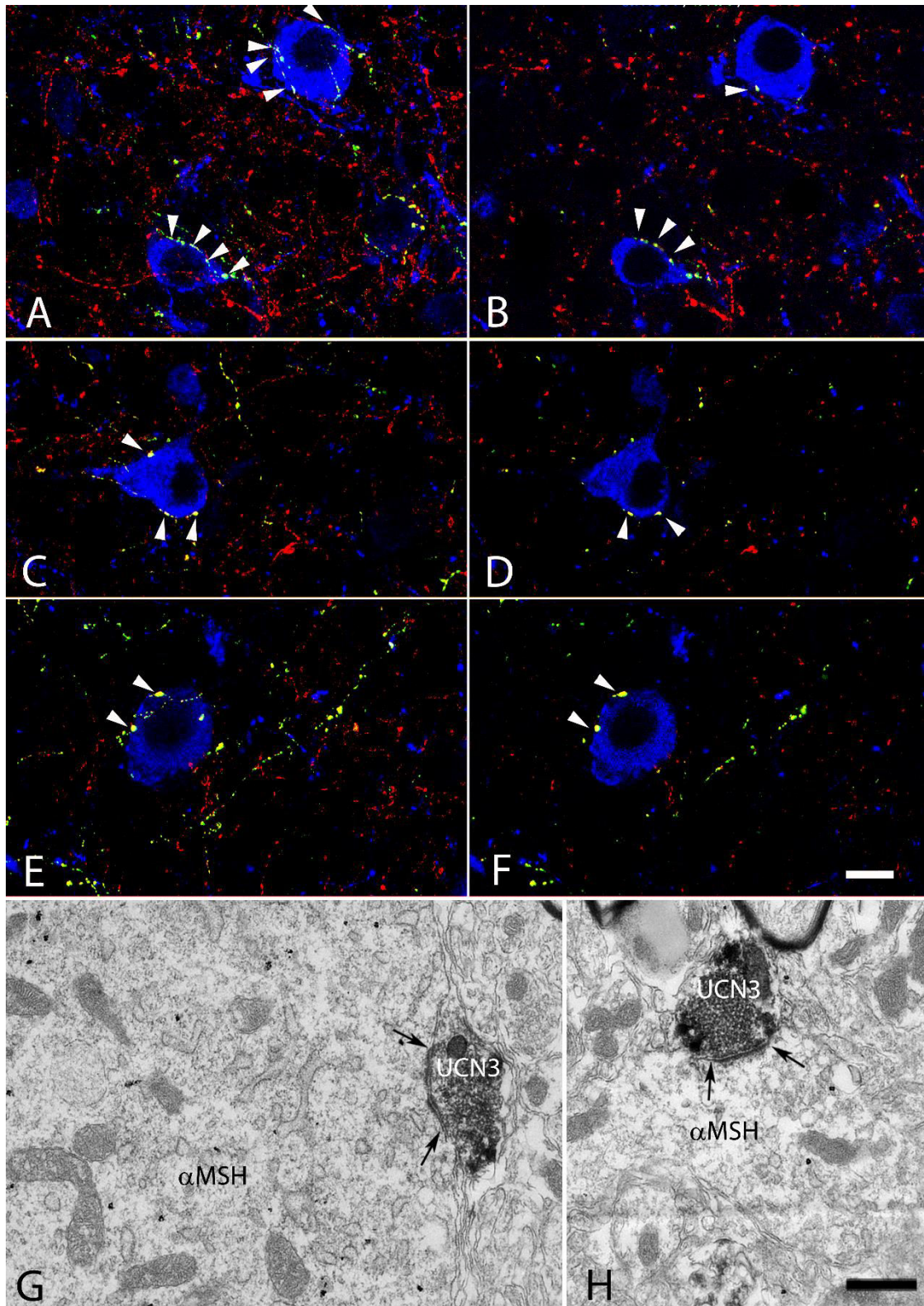
Figure 12 *Relationship of TRH/UCN3- containing axons and the α-MSH neurons in the ARC.*

*Triple-labeled immunofluorescent detection of the urocortin 3 (UCN3) - (green), thyrotropin-releasing-hormone-immunoreactive (TRH-IR) (red) axons and alpha-melanocyte-stimulating hormone (α-MSH) - (blue) neurons in the arcuate nucleus (ARC). The TRH/UCN3 axons contacted more than half of the α-MSH neurons (**A-F**) in the lateral part of ARC. Arrows point*

*to the double-labeled axon varicosities on the surface of α-MSH neurons (**A-F**). (**A**), (**C**) and (**E**) represent projections of 24 (**A**) or 8 (**C** and **E**) 0.8μm thick optical slices, while (**B**), (**D**) and (**F**) show a single 0.8 μm thick optical slice. Electron micrographs (**G, H**) illustrate synaptic associations (arrows) between α-MSH-IR neurons and UCN3-IR terminals in the ARC. The α-MSH -IR perikaryon (**C**) and dendrite (**D**) are labeled with highly electron dense gold–silver granules, while the UCN3-IR terminals are recognized by the presence of the electron dense diaminobenzidine chromogen. Asymmetric types of synapses were observed between UCN3-IR axon varicosities and the α-MSH-IR profiles. Arrows (**G, H**) point to the synapses. Nu, nucleus; Scale bar on (**F**) = 10 μm and corresponds to (**A-E**), (**H**) = 0.25 μm and corresponds to (**G**).*

IV.4 Relationship between TRH-IR axons and histaminergic neurons in the subnuclei of the TMN

Histamine-IR perikarya and dendrites were observed exclusively in the TMN, as it was previously described [107, 108]. Large, multipolar histamine-IR neurons were distributed in all five subnuclei (E1-5) of the TMN, forming the largest cell cluster in the E2 subnucleus close to the lateral surface of the hypothalamus (**Fig. 13-15**). Perikarya of the histamine-IR neurons in the E1 and E2 subnuclei were densely clustered, while the histamine-IR neurons in the E3-E5 subnuclei were more loosely organized (**Fig. 13-15**). TRH-IR neurons were also observed in the TMN, but almost exclusively in the E4 subnucleus (**Fig. 13-15**). Compared to the number of histamine-IR neurons in this subdivision, however, TRH neurons were far less abundant. Only scattered TRH-IR neurons were observed in the E1-E3 and E5 subnuclei.
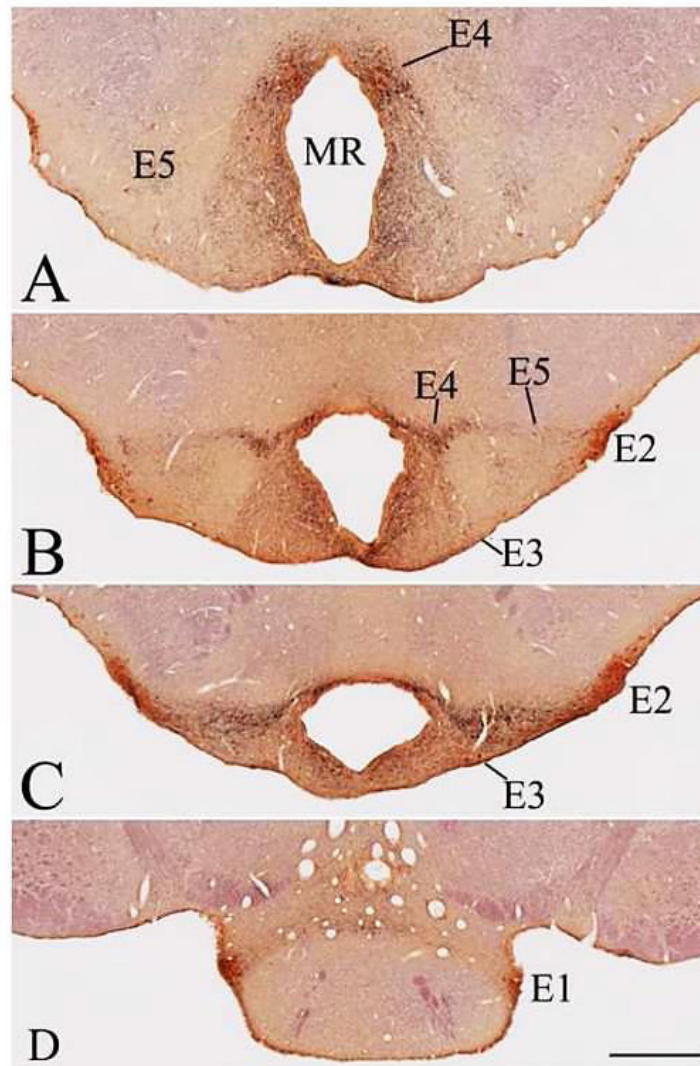
Figure 13 *Distribution of the TRH-IR elements (black) and the histamine-IR neurons (brown) in the subnuclei of the TMN in four different rostrocaudal levels of the TMN.*

The localization of the 5 subnuclei of the tuberomammillary nucleus (TMN) (E1-5) are labeled on the images. MR, mammillary recess; Scale bar = 500 µm.
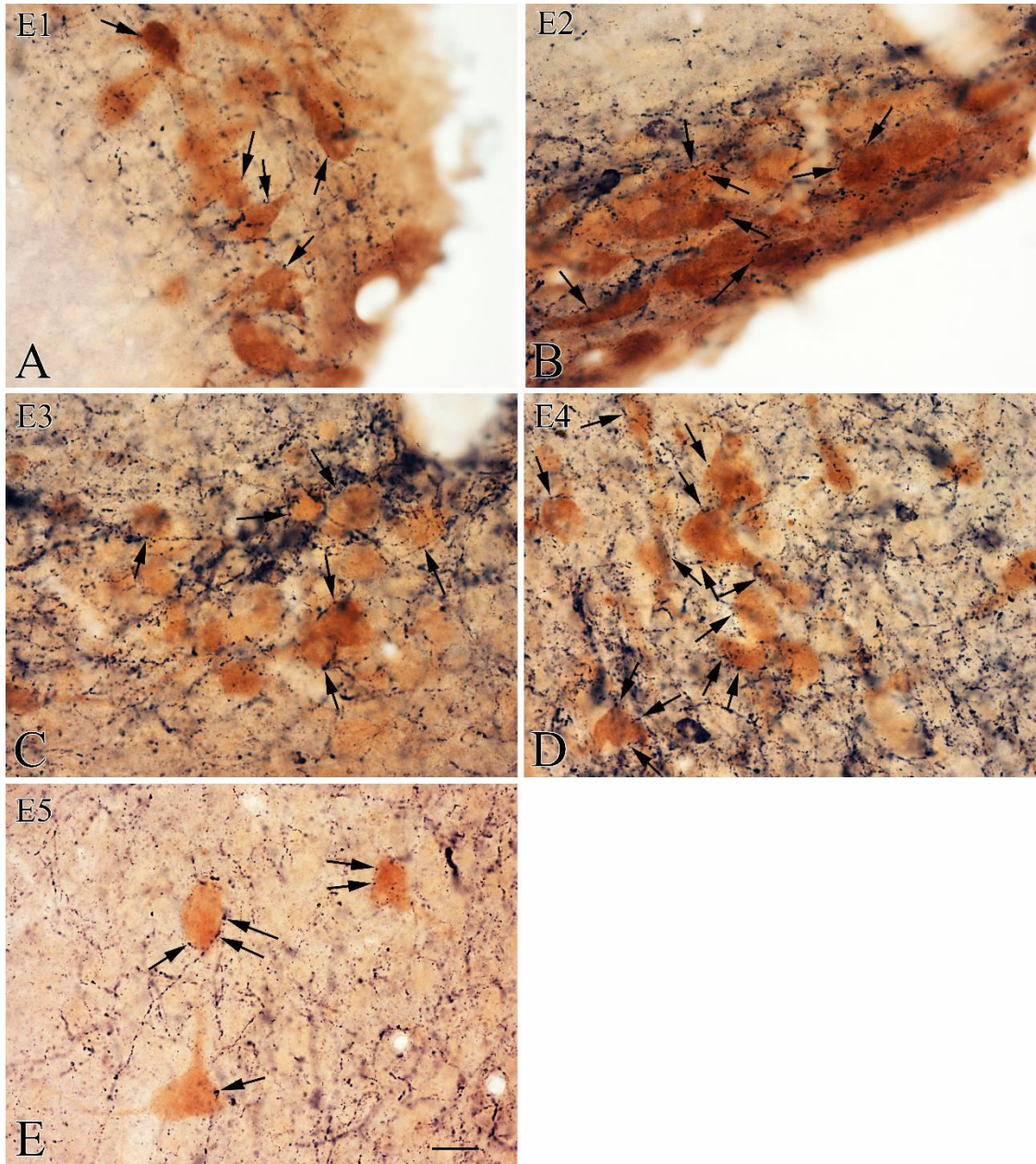
Figure 14 *Relationship of the TRH-IR (black) axon varicosities and the histamine-IR neurons (brown) in the 5 subnuclei of the TMN (**E1-5**).*

*Arrows point to thyrotropin-releasing-hormone-immunoreactive (TRH-IR) axon varicosities in juxtaposition to histamine-IR neurons. Especially high numbers of TRH-IR axons were observed in contact with the histamine-IR neurons in the E4 subnucleus (**D**). Scale bar = 20 μm.*

TRH-IR axons were found in all five subnuclei of the TMN, but the densest network of TRH-IR axons was observed in the E4 subnucleus (**Fig. 13, 14, 15**). Quantitative analyses of the morphological interaction of TRH-IR varicosities and histamine-IR neurons in the subnuclei

of the TMN was performed on confocal microscopic Z-stacks of less than 1 µm thick optical slices of double-labeled fluorescent sections (**Fig. 15**)
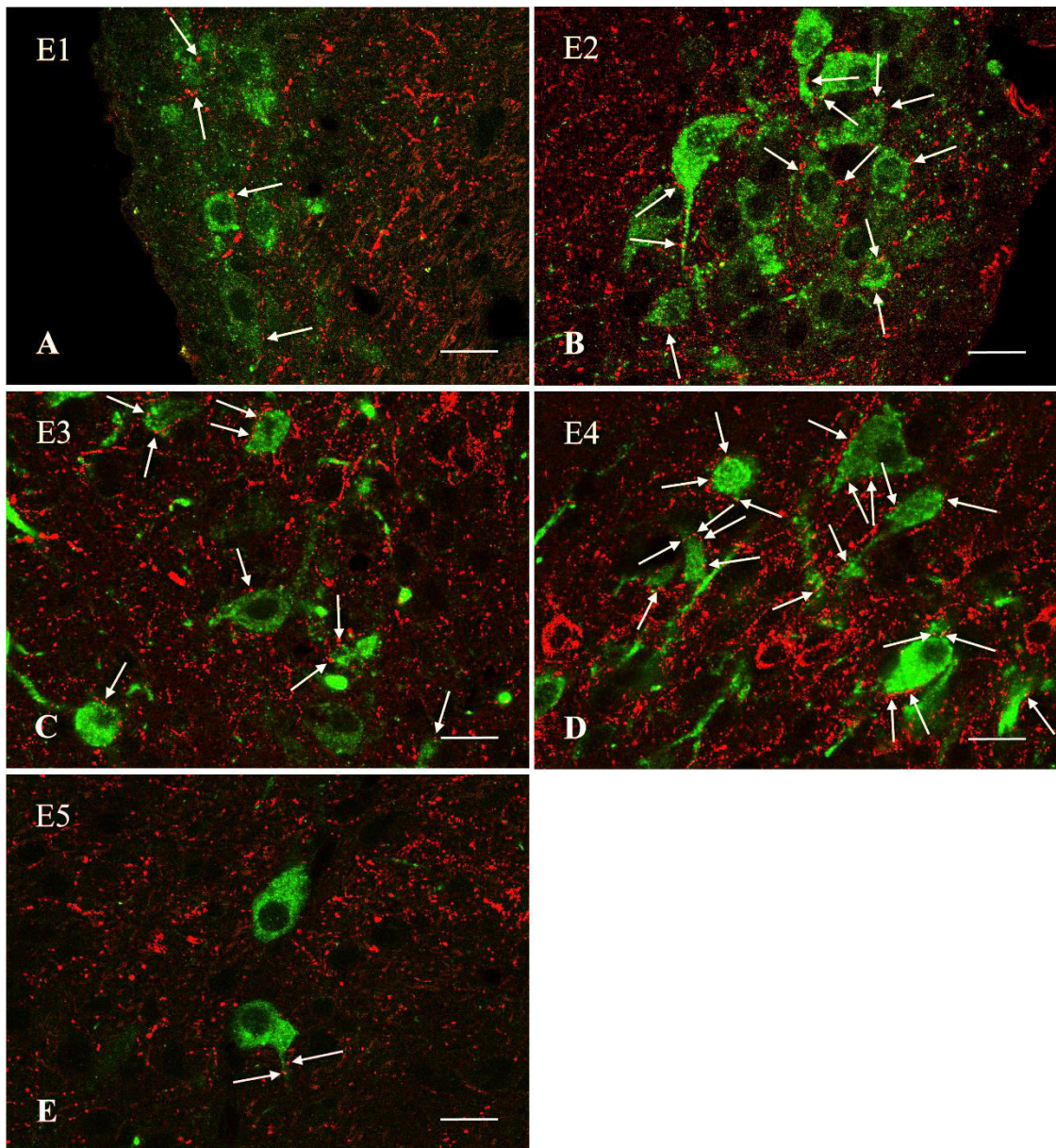
Figure 15 *TRH-IR (red) boutons innervate the histamine-IR neurons (green) (arrows) in the TMN.*

High power, confocal microscopic images of immunofluorescent preparations illustrate the juxtaposition of the thyrotropin-releasing hormone-immunoreactive (TRH-IR) varicosities and the histamine-IR neurons in the five subnuclei of the tuberomammillary nucleus (TMN) (E1-5). Arrows point to TRH-IR axon varicosities in juxtaposition to histamine-IR neurons. Images represent single optical sections with less than 0.8µm thickness. Scale bar = 20 µm.

The results of the analyses are summarized in **Table 6**. TRH-IR axon varicosities were observed on the surface of all histamine-IR neurons in the E4 subnucleus. An average of

27.0±1.2 varicosities per histamine-IR neurons were counted in this subnucleus (**Fig. 15D**). Similarly, all histamine-IR neurons were contacted by TRH-IR axon varicosities in the E5 subnucleus (**Fig. 15E**), but fewer TRH-IR varicosities (P<0.001) were observed on the surface of these cells (7.9±0.5). A dense TRH-IR innervation of E2 and E3 subnuclei (**Fig. 15B, C**) was observed, but somewhat fewer (P<0.001) histamine-IR neurons appeared to be contacted in these subnuclei; 93.9±0.9% in E2 and 92.1±1.3% in E3, averaging 6.3±0.2 and 6.8±0.2 TRH-IR varicosities per histamine-IR neuron in each subnucleus, respectively. A less frequent interaction between TRH-containing axon terminals and histamine-IR neurons was observed in the E1 subnucleus (**Fig. 14A, 15A**), where only 85.7±0.9% of the histamine-IR neurons (significantly less than all other groups P<0.001) were contacted by an average of 4.0±0.2 TRH-IR axon varicosities/innervated cells (significantly less than in all other groups P<0.001). At ultrastructural level, TRH-IR nerve terminals, labeled with electron dense DAB reaction product, were observed to established membrane appositions with histamine-IR perikarya and dendrites, recognized by the presence of highly electron dense immunogold-silver particles distributed throughout the labeled structures (**Fig. 16**). The juxtaposed TRH-IR terminals and histamine-IR neurons were tracked through series of ultrathin sections. Both asymmetric type (**Fig. 16A, B, F, G**) and symmetric type (**Fig. 16C, D, E, H**) synaptic specializations were observed on both perikarya and dendrites of histamine-synthesizing neurons. Analysis of 56 synapses between histamine neurons and TRH-IR terminals revealed 35 asymmetric and 14 symmetric type synaptic associations. For 7 of the identified synapses, the specific type could not be unequivocally determined.
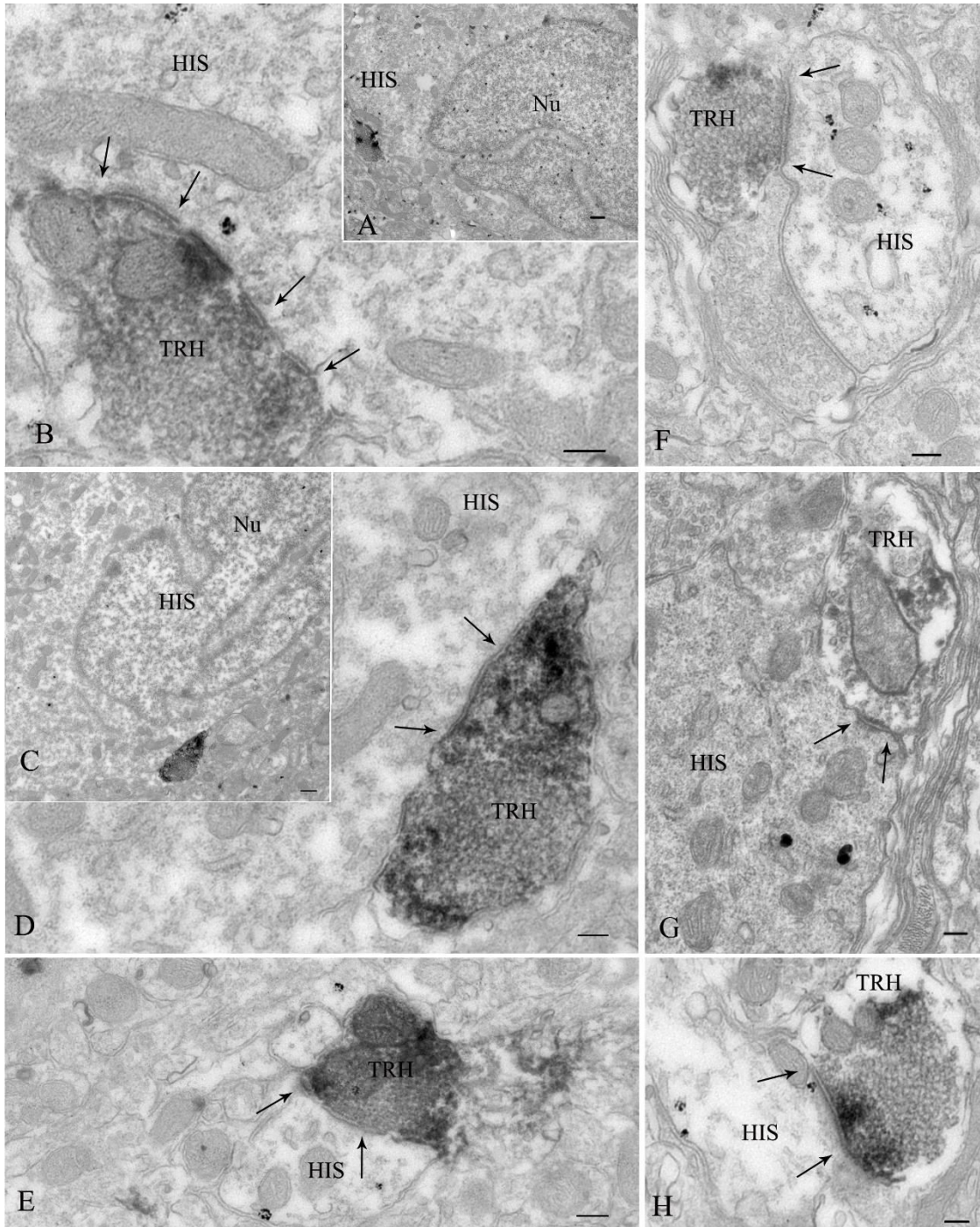
Figure 16 *Electron micrographs show synaptic associations (arrows) between histamine- IR neurons and TRH-IR terminals in the TMN.*

*The histamine- immunoreactive (IR) perikarya and dendrites are labeled with highly electron dense gold–silver granules, while the thyrotropin-releasing hormone (TRH)-IR terminals are recognized by the presence of the electron dense diaminobenzidine (DAB) chromogen. Medium-power image illustrates an asymmetric type synapse established between a TRH-IR axon varicosity and a histamine-IR perikaryon (**A**) shown in greater detail in (**B**). A symmetric type axosomatic synapse is shown in (**C, D**). High-power magnification images show asymmetric (**F, G**) and symmetric (**E, H**) axodendritic synapses between TRH and histamine-*

*IR structures. Arrows point to the synapses. HIS, histamine-IR structure; Nu, nucleus; TRH, TRH-IR structure; Scale bars=0.1 μm in (**B, D-H**); 1 μm in (**A, C**).*

Table 6 *Quantitative analysis of the juxtaposition of TRH-IR axon varicosities and histamine-IR neurons in the 5 TMN (E1-5).*

	E1	**E2**	**E3**	**E4**	**E5**
Percentage of histamine-IR neurons contacted by TRH-IR axons	85.7±0.9 *a*	93.9±0.9 *b*	92.1±1.3 *c*	100.0±0.0 *d*	100.0±0.0 *d*
Number of TRH varicosities/histamine-IR neuron	4.0±0.2 *a*	6.3±0.2 *e*	6.8±0.2 *e*	27.0±1.8 *f*	7.9±0.5 *e*

a significantly different from E2, E3, E4, E5; *b* significantly different from E1, E3, E4, E5

c significantly different from E1, E2, E4, E5; *d* significantly different from E1, E2, E3

e significantly different from E1, E4; *f s*ignificantly different from E1, E2, E3, E5; *P*<0.05

59

V.   Discussion

V.1   Anatomy of the NO system in the parvocellular part of the PVN and its potential interaction with the endocannabinoid system

NPY is one of the most potent orexigenic molecules known, its effects on energy expenditure and food intake are at least in part mediated in the PVN [3]. During fasting, when the hunger drive is increased, the NPY level is also increased in the PVN, and administration of NPY directly into this nucleus of sated rats markedly increases food intake and decreases energy expenditure [109]. However, little information is available about how NPY exerts these effects on energy homeostasis within the PVN. Electrophysiological data from our laboratory [49] demonstrated that retrograde signaling systems are involved in the mediation of the NPY effects within the PVN. One of the retrograde signaling systems involved in this process is the endocannabinoid system [49]. Since the interaction of the endocannabinoid and the NO system was demonstrated in the regulation of hippocampal axon terminals [57], we have studied whether the NO may also serve as retrograde transmitter in the PVN.

By ultrastructural studies, we demonstrated that both nNOS and the major NO receptor, sGCα1, is present in both pre- and postsynaptic sites within the parvocellular subdivisions of the PVN. In many instances, the nNOS-immunoreactivity was associated to the postsynaptic density of synapses. These data indicate that similarly as it was described in the hippocampus [56], NO may have both anterograde and retrograde transmitter function. Later, electrophysiological data from our laboratory supported this finding. It was shown that inhibition of nNOS completely prevented the inhibitory effect of NPY on the inhibitory inputs of the parvocellular neurons, but alone had no effect on the excitatory inputs of the parvocellular neurons [49].

As electrophysiological data from our laboratory showed that inhibition of either the endocannabinoid or the NO system completely prevented the effect of NPY on the inhibitory inputs [49], we hypothesized that the two systems regulate the very same synapses. Therefore, we have studied whether the elements of the two systems are associated to the same synapses in the parvocellular part of the PVN.

Our quadruple-labeling immunofluorescent data showed that both glutamatergic and GABAergic CB1-containing axon varicosities juxtapose to nNOS-containing dendrites of the parvocellular neurons in the PVN. In addition, the co-localization of nNOS and the endocannabinoid-synthesizing DAGLα was observed in the dendrites of the parvocellular neurons. These data further suggested the interaction of the two signaling systems in the regulation of the very same synapses of the parvocellular neurons. Since light microscopy

cannot prove that the juxtaposed profiles form synaptic associations, we have studied the association of the two systems at ultrastructural level. Using electron microscopy, we have found that in many cases nNOS-immunoreactivity was associated to the postsynaptic side of the synapse formed by a CB1-containing axon varicosity. This type of arrangement of nNOS and CB1 was observed in association to both symmetric and asymmetric type synapses suggesting that the two signaling systems may interact not only in the regulation of the inhibitory, but also in the regulation of the excitatory synapses of the parvocellular neurons of the PVN. Since inhibition of endocannabinoid system alone prevented the effect of NPY on the excitatory input of parvocellular neurons, but inhibition of nNOS alone had not effect on these inputs, to test the potential interaction of the two signaling systems in the excitatory synapses of the parvocellular neurons, our laboratory studied whether co-administration of the subthreshold doses of the CB1 antagonist AM251 and the nNOS inhibitor together can inhibit the effect of NPY on the excitatory synapses of parvocellular neurons. The results of this electrophysiological experiments showed that co-administration of subthreshold dose of AM251 and NPLA completely prevented the NPY induced inhibition of the excitatory inputs of the parvocellular neurons proving the functional interaction of the two signaling systems in the excitatory synapses.

Thus our morphological data demonstrate that the NO system is utilized as both anterograde and retrograde transmitter within the parvocellular part of the PVN and regulates both excitatory and inhibitory connections in this brain region. Furthermore, our data demonstrate the anatomical basis of the interaction of the NO and endocannabinoid systems in the regulation of the inputs of the parvocellular PVN neurons. The functional importance of these findings was demonstrated by the patch clamp electrophysiological observations of our laboratory.

V.2   The endocannabinoid and the NO systems of the PVN mediate different effects of NPY on the energy homeostasis

To determine the importance of the endocannabinoid and NO systems of the PVN in the mediation of NPY induced changes of the energy homeostasis, *in vivo* experiments were performed. Inhibition of nNOS within the PVN completely prevented the potent stimulatory effect of the intraPVN administration of NPY on the food intake. Furthermore, inhibition of nNOS decreased food intake even if NPY was not administered exogenously, but the endogenous NPY release was increased in fasted animals within the PVN before food was reintroduced. These data strongly suggest an important role for NO in the regulation of food intake, but only in the presence of increased release of NPY in the PVN. In addition, antagonizing nNOS with NPLA prolonged the stimulatory effects of NPY on locomotor

activity without influencing the RER. Since the NPY-induced increase in RER paralleled the NPY-induced increase in locomotor activity, it raised the possibility that the NPY-induced increase in carbohydrate utilization was induced by increased locomotor activity and not a direct, central effect of NPY. However, NPLA treatment only prolonged the NPY-induced increase in locomotor activity without influencing substrate utilization, suggesting that the effects of NPY on locomotor activity and substrate utilization are mediated via separate, central mechanisms within the PVN.

In contrast, antagonizing the endocannabinoid signaling system had no effect on food intake, as demonstrated by the absence of a response when a CB1 antagonist was administered simultaneously with NPY directly into the PVN, or during fasting. Nevertheless, endocannabinoid signaling would appear to be involved in the mediation of the NPY-induced effect on energy expenditure, as inhibition of CB1 prevented ~50% of the NPY-induced decrease in energy expenditure. This observation is similar to the effect of NPY on glutamatergic synapses, which can be blocked by AM251 but not by NPLA. Therefore, we hypothesize that NPY inhibits energy expenditure via inhibition of the excitatory inputs of the parvocellular neurons.

In contrast to the endocannabinoid system, NO is utilized as both a retrograde and anterograde transmitter in the PVN. While the nature of patch clamp methodology allowed the examination of NO as retrograde transmitter, *in vivo* inhibition of nNOS in the PVN blocked both anterograde and retrograde NO transmission. Since all of the retrograde transmitter mediated effects of NPY could be also prevented in patch clamp studies with administration of the CB1 antagonist AM251, but the *in vivo* effects of NPY on the food intake [49] and locomotor activity were influenced only by local inhibition of NO signaling within the PVN, we hypothesize that the effects of NPY on food intake and locomotor activity are mediated by local neuronal circuits utilizing NO as an anterograde transmitter.

Interestingly, inhibition of the NO synthesis in the PVN had different effects on NPY-induced locomotor activity in the presence or absence of food. When food was not available, NPLA prolonged the NPY-induced increase in locomotor activity, while in the presence of food; NPLA completely blocked NPY-induced locomotor activity. Therefore, it is likely that NPY stimulates locomotor activity via different mechanisms in the presence or absence of food.

Thus our data demonstrate that the endocannabinoid system is involved in the mediation of the effects of NPY on the energy expenditure, while the NO system is involved in the regulation of food intake by NPY. In addition, the presented data indicate that the effect of NPY on the locomotor activity, RER, food intake and energy expenditure are mediated by different neuronal circuits of the PVN.

V.3   Presence of the MCT8 protein in axon terminals of the hypophysiotropic TRH axons in the ME of the rat

MCT8 is considered to be the predominant, neuronal T3 transporter, and mutations of this gene in humans are characterized by a severe neurologic phenotype [62]. Importantly, absence of functional MCT8 also results in increase of circulating thyroid hormone levels in both humans and rodents [62, 64] indicating the importance of MCT8 in the feedback regulation of the HPT axis. We demonstrated that in the median eminence, MCT8 is present not only in the tanycytes, but also in the hypophysiotropic axon terminals. Using double-labeling immunofluorescence, we showed that among these hypophysiotropic terminals, specifically the axon terminals of the hypophysiotropic TRH neurons also contain MCT8. As the transport of T3 through the blood-brain-barrier is not efficient and T4 cannot bind to the nuclear thyroid hormone receptors [27], local thyroid hormone activation is necessary for the feedback regulation of the thyroid hormones. As axon terminals of the hypophysiotropic TRH neurons in the external zone of the ME lie in close proximity to the endfeet processes D2 expressing tanycytes [110] the observation that practically all hypophysiotropic axon terminals in the ME express MCT8 indicate that T3 released from tanycytes could readily accumulate in the terminals of hypophysiotropic TRH neurons and then reach the nucleus of these cells by retrograde transport. Although the machinery driving the retrograde transport of T3 is yet unknown, fast retrograde axonal transport of biologically active molecules is not unprecedented [111]. Since the perikarya of the hypophysiotropic TRH neurons are located relatively far from the tanycytes, it is likely that the retrograde axonal transport of T3 is the main route of T3 trafficking between tanycytes and hypophysiotropic TRH perikarya.

T3 in the ME originates from two sources: from the peripheral circulation and from the tanycytes. The ME is located outside of the blood-brain-barrier [26], thus, T3 can enter freely to the extracellular space of the ME from the fenestrated capillaries of the hypophyseal portal circulation [26]. In addition, tanycytes can take up T4 from the CSF, from the blood stream or from the extracellular space of the median eminence [112]. As tanycytes express D2, this enzyme can activate the T4 by converting it to the active T3 and release this hormone to the ME [27]. The changes of peripheral thyroid hormone levels do not regulate the activity of D2 in the tanycytes [113], therefore, under basal conditions tanycytes simply convert the changes of peripheral T4 concentration to changes of median eminence T3 concentration. Under certain physiological and pathophysiological conditions, however, the D2 activity of tanycytes is regulated. For example, in response to the administration of bacterial lipopolysaccharide (LPS), a model of infection, the D2 activity of tanycytes is markedly increased independently from the changes of circulating thyroid hormone levels [114, 115], inducing local

hypothyroidism in the ARC-ME region [116]. This local increase of T3 concentration is necessary for the development of infection induced central inhibition of the HPT axis [117]. Thus the involvements of tanycytes in the feedback regulation of the hypophysiotropic TRH neurons provide an additional regulatory element in the central control of the HPT axis [117].

Thus, the identification of MCT8 in the axon terminals of the HPT axis resulted in the development of a novel model of the feedback regulation of the HPT axis [27] that can answer several earlier unresolved questions. For example, it was unclear earlier, why the circulating thyroid hormone levels of the D2 KO mice are normal or why the non-hypophysiotropic TRH neurons are not responsive to the changes of peripheral thyroid hormone levels despite the fact that these cells also contain thyroid hormone receptors [27].

Thyroid hormone also plays a critical role in the regulation of other neuroendocrine axes including, the reproductive axis, adrenal axis and growth-hormone (GH) secretion [118-123]. The observation that practically all hypophysiotropic axon terminals in the ME express MCT8 indicates the ME can be the main source of T3 that regulates these hypophysiotropic axes. Indeed, tanycytes are known to regulate the hypophysiotropic GnRH neurons via modulation of T3 availability in seasonal animals [124].

V.4   TRH/UCN3 neurons of the perifornical area/BNST region innervate the α-MSH neurons of the ARC

Previous data from our laboratory demonstrated that TRH and UCN3 are co-synthetized in the neurons located in the perifornical area/BNST region [67]. To determine whether TRH/UCN3 neurons may regulate food intake *via* orexigenic and/or anorexigenic neurons in the ARC, the relationship between double-labeled TRH/UCN3 axons and the NPY or α-MSH neurons was studied in the ARC using triple-labeling immunofluorescence. The double-labeled axons contacted only a minority of NPY neurons, making it unlikely that TRH/UCN3 neurons have a major, direct influence on this orexigenic neuron population. In contrast, more than half of the anorexigenic POMC were contacted by multiple TRH/UCN3 axon varicosities. Since the vast majority of UCN3 axons also contained TRH in the ARC, we used UCN3 as a marker of TRH/UCN3 fibers when the relationship of these axons and the α-MSH-IR neurons were studied at ultrastructural level. Double-labeling immuno-electron microscopy revealed that synaptic associations were frequently observed between the UCN3-IR axons and α-MSH-IR perikarya and dendrites. In all cases, the synaptic associations were asymmetric type, indicative of the excitatory nature of this synaptic communications.

Since central administration of both TRH and UCN3 have a similar effect to reduce food intake as do activation of POMC neurons [3, 65, 125], we hypothesized that both peptides would stimulate POMC neurons and that their co-administration would have an additive

effect. Therefore, based on the presented morphological data, our laboratory performed patch clamp electrophysiological studies to determine the role of TRH and UCN3 in the regulation of the POMC neurons. The data of these experiments showed that the two peptides had opposite effects on the POMC neurons. As expected, UCN3 markedly depolarized the POMC neurons by acting on CRF type 2 receptor (CRFR2) and increased the spontaneous firing frequency of these cells demonstrating that UCN3 activates the POMC neurons.

In contrast, TRH treatment caused hyperpolarization of POMC neurons and decreased the firing frequency of these cells. The effect of TRH on the membrane potential of POMC neurons was prevented by tetrodotoxin, a compound that blocks the synaptic inputs, suggesting that the inhibitory effect of TRH on the POMC neurons is indirect. Simultaneous administration of TRH with UCN3 completely prevented the effects of UCN3 on the membrane potential and the firing of POMC neurons. The effect of TRH on the UCN3 induced depolarization was preserved even in the presence of tetrodotoxin, indicating that TRH can act directly on POMC neurons; and antagonizes UCN3-induced stimulation rather than having an additive effect.

The antagonistic effect of the two peptides was surprising as TRH has stimulatory effects on many cell types [126-128]. However, Ballerini et al. [129] observed a similar phenomenon in pyramidal cells of the hippocampal CA1 region, showing that TRH has no effect on the membrane potential of those cells but prevented the effect of an another transmitter [129]. The highly divergent effects of TRH on target neurons may be due to differential expression of the two TRH receptors, TRHR1 and 2, in these cell populations. Since specific antagonists of TRH receptors are unavailable, the receptor specificity of the TRH effect on POMC neurons could not be detected.

Our data suggest, however, that while UCN3 may inhibit food intake by stimulating POMC neurons of the ARC, TRH may prevent or terminate the effect of UCN3. These data are especially interesting because the two, anorexigenic peptides are released from the very same axon terminals and exerted antagonistic effects on the POMC neurons. So far, the physiological importance of this interaction is not yet clear. We hypothesize, however, that the differential expression and release of the two peptides enables TRH/UCN3 neurons to exert distinct effects on the POMC neurons under different physiological or pathophysiological conditions. Further studies using optogenetics may help to understand whether the length, pattern or the frequency of the firing of TRH/UCN3 neurons differentially alter the release of the two peptides, and whether the two peptides are released simultaneously from the axons or independently or sequentially of each other. In the latter case, TRH might terminate the UCN3 induced excitation of POMC neurons.

Since stress increases the synthesis of UCN3 in perifornical neurons [25] and causes anorexia *via* activation of the POMC neurons of the ARC [25], based on our current data, we raise the possibility that TRH/UCN3 neurons of the perifornical area/BNST region mediate the effects of stress on POMC neurons. However, further studies will be necessary to understand the importance of this pathway in the stress-induced activation of the POMC neurons, and to identify the pathways activating the TRH/UCN3 neurons during stress.

V.5   Relationship between TRH-IR axons and histaminergic neurons in the subnuclei of the TMN

Histamine producing neurons are located in the posterior hypothalamus, in the TMN [108]. Histamine serves as a neurotransmitter in the brain and plays important role in the regulation of body weight. Numerous previous studies confirmed that the central administration of histamine can reduce food intake [70, 130, 131]. The mechanisms by which histaminergic neurons are integrated into the central mechanisms for weight regulation are not completely known, but the observation that the anorexic effects of TRH on food intake can be attenuated by preventing the synthesis of histamine raises the possibility that non-hypophysitropic TRH-synthesizing neurons may comprise at least one of the feeding related inputs of the histaminergic neurons. We demonstrated that TRH-IR axons densely innervate all five subdivisions of the TMN and establish numerous, close appositions with histaminergic neurons in each subdivision.

Ultrastructural analysis showed that TRH-IR axons frequently establish synaptic associations with both the perikaryon and dendrites of histamine-IR neurons. While both symmetric and asymmetric type synapses were observed, the number of asymmetric type synapses was almost 3 times higher than the number of symmetric type specializations. Since, the asymmetric type synaptic association is considered a characteristic feature of the excitatory neuronal connections [132] the data suggest that TRH exerts primarily stimulatory effect on the histaminergic neurons. This is in agreement with the earlier findings showing that, central administration of TRH increases histamine concentration in the TMN [133] and has a depolarizing effect on histaminergic neurons [134]. TRH can exert its effects *via* TRHR1 or TRHR2 receptors or both of them [135]. Although single cell PCR has demonstrated both types of receptors in some of the histaminergic neurons [134], but using immunocytochemistry, only TRHR2 has been visualized [133]. Due to the lack of selective TRHR antagonists, functional studies could not be performed to determine the receptor type mediating the effects of TRH on the histaminergic neurons.

66

How symmetric type TRH synapses contribute to the regulation of histaminergic neurons requires further study, but raises the possibility that the origin of TRH neurons that innervate the TMN neurons is diverse.

Juxtaposition of TRH-IR axons to histamine-IR neurons was observed in all subnuclei of the TMN, but the densest innervation pattern was observed in the dorsomedially located E4 subnucleus. Here, approximately four times more TRH-IR axons were observed on the surface of the innervated histamine-IR neurons than any other TMN subnucleus. The physiological significance for this innervation pattern is currently unclear, as very little is known about the functional differences of the various TMN subnuclei. Early anatomical studies suggest that all TMN subnuclei have similar projection patterns. Namely, tract tracing studies showed that retrogradely labeled histaminergic neurons were equally observed in all subnuclei after tracer injection into the studied projection fields [136] indicating that they may subserve similar functions. Restraint stress, insulin-induced hypoglycaemia and foot shock, however, induce neuronal activation preferentially in the E4 and E5 TMN subnuclei [137] suggesting functional heterogenity. Furthermore, Mahia et al. [138] demonstrated that electrolytic lesions of the TMN subnuclei have differential effects on the food intake, such that lesions of the ventral E1 and E2 subnuclei result in hyperphagia, whereas similar lesions of E3 and E4 subnuclei have no effect. Electrolytic lesions not only damage neuronal perikarya, however, but also axons of passage. Since the caudal ARC is closely juxtaposed to the E3 and E4 subnuclei, ablation of the axons emanating from the ARC might have confounded interpretation of the data. Further studies using focal injections of TRH into the different subnuclei of the TMN, therefore, will be necessary before definitive conclusions can be rendered about the preferential role of any of the TMN subnuclei in the mediation of the anorexigenic effects of TRH.

In addition to the effects of TRH on food intake, TRH also participates in the central control of thermoregulation through effects independent of elevations in circulating thyroid hormone levels. Without affecting circulating T3 levels, intracerebroventricular administration of TRH increases rectal temperature and temperature of BAT that can be prevented by pretreatment with antibodies to the type 1 TRH receptor [139]. In addition, exposure of the total TRH KO mouse to cold results in hypothermia that cannot be fully rescued by restoring thyroid hormone levels [140] Since bilateral denervation of the sympathetic nerves innervating BAT or the administration of β-adrenergic antagonists markedly attenuate the thermogenic response of centrally administered TRH [139], the effects of TRH are presumably mediated through the sympathetic innervation of BAT. Activation of histaminergic neurons also increases thermogenesis through activation of the sympathetic innervation to BAT [70]. Thus, it is

67

possible that the TRH innervation of histaminergic neurons in the TMN may also mediate the thermogenic effect of this peptide on BAT.

Histaminergic neurons in the TMN may also mediate the effect of TRH on wakefulness. Both TRH and histamine are known to increase arousal [141, 142], and inhibition of histamine synthesis by α-FMH blocks the effect of the TRH analog, montirelin, to induce arousal, suggesting that the effect is mediated by histaminergic neurons. Since wakefulness results in c-Fos activation in all TMN subnuclei [143] it is possible that all subnuclei may be involved in the mediation of the effects of TRH on arousal.

Based on the described anatomical connections, we are currently performing tract tracing studies to identify the sources of the TRH-IR innervation of the histaminergic neurons. After identification of the TRH cell populations innervating the histaminergic neurons, we plan to perform optogenetic or chemogenetic studies to study the role of these TRH cell populations in the regulation of energy homeostasis.

VI. New scientific results

VI.1 [C1-C5] Thesis I

The ultrastructural localization of the elements of the nitric oxide transmitter system in the parvocellular part of the PVN indicate that NO is utilized as both anterograde and retrograde neurotransmitter in this brain region.

The nNOS and the sGC has both pre- and postsynaptic localization in the parvocellular part of the PVN indicating that the NO may serve as both anterograde and retrograde transmitter in this brain region.

VI.2 [C1-C5] Thesis II

NO and the endocannabinoid systems are associated to the same synapses of the parvocellular neurons of the PVN.

nNOS is associated to the postsynaptic side of a population of the synapses formed by CB1-IR terminals on the parvocellular neurons. These data indicate that the NO and the endocannabinoid systems may interact in the regulation of presynaptic terminals in the parvocellular part of the PVN.

VI.3 [C1-C5] Thesis III

The endocannabinoid and the NO systems of the PVN are involved in the mediation of the NPY induced regulation of energy homeostasis

Both transmitter systems have critical, but different role in the mediation of the effects of NPY on the energy homeostasis. While the NO system of the PVN mediates the effects of NPY on the food intake, the endocannabinoid system of this nucleus is involved in the mediation of the NPY induced regulation of energy expenditure. Furthermore, data of our group indicates that different neuronal circuits of the PVN are involved in the regulation of food intake, energy expenditure and locomotor activity by NPY.

VI.4 [J1] Thesis IV

MCT8 thyroid hormone transporter presents in the axon terminals of the hypophysiotropic TRH neurons.

MCT8 is present in the hypophysiotropic axon terminals in the external zone of the ME. Furthermore, specifically the axon terminals of the hypophysiotropic TRH neurons also contain this thyroid hormone transporter. Based on this finding, a novel concept of the thyroid hormone feedback regulation of the hypophysiotropic TRH axons was established.

VI.5   [J2] Thesis V

The TRH/UCN3 neurons of the perifornical area/BNST region innervate the feeding related neuronal groups of the ARC.

The axons of the TRH/UCN3 neurons juxtapose to only the minority of the NPY neurons of the ARC, but contacts more than half of the α-MSH neurons of the nucleus. At ultrastructural level, the TRH/UCN3 axons establish asymmetric type synaptic specializations with the α-MSH neurons.

VI.6   [J3] Thesis VI

TRH-containing axons innervate the histaminergic neurons in all subnuclei of the TMN.

TRH-IR axons densely innervate the histaminergic neurons in all subnuclei of the TMN, and establish synaptic specializations on the surface of these neurons. The majority of the synaptic contacts were found to be asymmetric type, but symmetric synapses were also found between the two systems.

Journal and conference publications of the Author

VII.   Author's journal publications

*These authors have contributed equally to the work.

[J1] *Kallo, I; Mohacsik, P; Vida, B; Zeold, A; Bardoczi, Z; Zavacki, AM;* **Farkas, E***; Kadar, A; Hrabovszky, E; Arrojo, e Drigo R; et al.*

A Novel Pathway Regulates Thyroid Hormone Availability in Rat and Human Hypothalamic Neurosecretory Neurons PLOS ONE 7 : (6) Paper: e37860 , 16 p. (2012)

[J2] *Zoltán Péterfi*[*]*,* **Erzsébet Farkas**[*]*, Kata Nagyunyomi-Sényi,Andrea Kádár, Szenci Ottó, András Horváth, Tamás Füzesi, Ronald M. Lechan, Csaba Fekete*

Role of TRH/UCN3 neurons of the perifornical area/ bed nucleus of stria terminalis region in the regulation of the anorexigenic POMC neurons of the arcuate nucleus in male mice and rats BRAIN STRUCTURE and FUNCTION Accepted (2017)

[J3] *Sarvari, A*;* **Farkas, E*;** *Kadar, A; Zseli, G; Fuzesi, T; Lechan, RM; Fekete, C*

Thyrotropin-releasing hormone-containing axons innervate histaminergic neurons in the tuberomammillary nucleus BRAIN RESEARCH 1488 pp. 72-80. (2012)

VIII.   Author's conference publications

[C1] *Zoltán Péterfi*, Imre Farkas*, Raphael Denis*,* **Erzsébet Farkas***, Motokazu Uchigashima, Masahiko Watanabe, Ronald M Lechan, Zsolt Liposits6, Serge Luquet and Csaba Fekete*

Endocannabinoid and Nitric Oxide Retrograde Signaling Systems in the Hypothalamic Paraventricular Nucleus Have a Critical Role in Mediating the Effects of Npy on Energy Expenditure Endocrine Reviews Volume 37, Issue 2 Supplement, April 2016

[C2] **<u>Erzsébet, Farkas,</u>** *Fekete, C; Lechan, RM.*

Subcellular localization of the components of the nitric oxide system in the hypothalamic paraventricular nucleus of mice Phd Proceedings Annual Issues Of The Doctoral School Faculty Of Information Technology And Bionics 10 pp. 29-32. (2015)

[C3] **Erzsébet, Farkas,** *Fekete, C; Lechan, RM.*

Structural and functional characterization of the retograde signaling system in the hypothalamic paraventricular nucleus Phd Proceedings Annual Issues Of The Doctoral School Faculty Of Information Technology And Bionics 2014 pp. 15-18. (2014)

[C4] **Erzsébet, Farkas,** *Fekete, C; Lechan, RM.*

Subcellular localization of the components of the nitric oxide system in the hypothalamic paraventricular nucleus of mice Pázmány Péter Catholic University Phd Proceedings pp. 21-24. (2013)

[C5]**E. Farkas**, *R. M. Lechan, C. Fekete*

Subcellular localization of the components of the nitric oxide system in the hypothalamic paraventricular nucleus of mice. Society of Neuroscience (2012)

IX. Author's other publications

Wittmann, G; **Farkas, E**; *Szilvasy-Szabo, A; Gereben, B; Fekete, C; Lechan, RM*

Variable proopiomelanocortin expression in tanycytes of the adult rat hypothalamus and pituitary stalk. JOURNAL OF COMPARATIVE NEUROLOGY 525 : (3) pp. 411-441. (2017)

Farkas, I; Vastagh, C; **Farkas, E;** *Balint, F; Skrapits, K; Hrabovszky, E; Fekete, C; Liposits, Z*

Glucagon-Like Peptide-1 Excites Firing and Increases GABAergic Miniature Postsynaptic Currents (mPSCs) in Gonadotropin-Releasing Hormone (GnRH) Neurons of the Male Mice via Activation of Nitric Oxide (NO) and Suppression of Endocannabinoid Signaling Pathways. FRONTIERS IN CELLULAR NEUROSCIENCE 10 p. 214 (2016)

McAninch, EA; Jo, S; Preite, NZ; **Farkas, E;** *Mohacsik, P; Fekete, C; Egri, P; Gereben, B; Li, Y; Deng, Y; et al.*

Prevalent Polymorphism in Thyroid Hormone-Activating Enzyme Leaves a Genetic Fingerprint that Underlies Associated Clinical Syndromes. JOURNAL OF CLINICAL ENDOCRINOLOGY AND METABOLISM 100 : (3) pp. 920-933. (2015)

Singru, PS; Wittmann, G; **Farkas, E;** *Zseli, G; Fekete, C; Lechan, RM*

Refeeding-Activated Glutamatergic Neurons in the Hypothalamic Paraventricular Nucleus (PVN) Mediate Effects of Melanocortin Signaling in the Nucleus Tractus Solitarius (NTS) ENDOCRINOLOGY 153 pp. 3804-3814. (2012)

Farkas E, *Ujvarosi K, Nagy G, Posta J, Banfalvi G.*

Apoptogenic and necrogenic effects of mercuric acetate on the chromatin structure of K562 human erythroleukemia cells. TOXICOL IN VITRO. 1 pp:267-75. (2010)

References

1. Kopelman, P.G., *Obesity as a medical problem. Nature, 2000.* **404***(6778): p. 635-43.*

2. commission, E. *The fight against obesity Examples of EU projects in the field of nutrition and obesity. Available from:* ftp://ftp.cordis.europa.eu/pub/food/docs/nutrition_obesity_examples.pdf.

3. Schwartz, M.W., et al., *Central nervous system control of food intake. Nature, 2000.* **404***(6778): p. 661-71.*

4. Zhang, Y., et al., *Positional cloning of the mouse obese gene and its human homologue. Nature, 1994.* **372***(6505): p. 425-32.*

5. Lee, G.H., et al., *Abnormal splicing of the leptin receptor in diabetic mice. Nature, 1996.* **379***(6566): p. 632-5.*

6. Montague, C.T., et al., *Congenital leptin deficiency is associated with severe early-onset obesity in humans. Nature, 1997.* **387***(6636): p. 903-8.*

7. Farooqi, I.S., et al., *Clinical and molecular genetic spectrum of congenital deficiency of the leptin receptor. N Engl J Med, 2007.* **356***(3): p. 237-47.*

8. Bruning, J.C., et al., *Role of brain insulin receptor in control of body weight and reproduction. Science, 2000.* **289***(5487): p. 2122-5.*

9. Dawson, R., et al., *Attenuation of leptin-mediated effects by monosodium glutamate-induced arcuate nucleus damage. Am J Physiol, 1997.* **273***(1 Pt 1): p. E202-6.*

10. Horvath, T.L., et al., *Heterogeneity in the neuropeptide Y-containing neurons of the rat arcuate nucleus: GABAergic and non-GABAergic subpopulations. Brain Res, 1997.* **756***(1-2): p. 283-6.*

11. Kelly, J., et al., *GABA stimulation and blockade in the hypothalamus and midbrain: effects on feeding and locomotor activity. Pharmacol Biochem Behav, 1977.* **7***(6): p. 537-41.*

12. Chambers, A.P. and S.C. Woods, *The role of neuropeptide Y in energy homeostasis. Handb Exp Pharmacol, 2012(209): p. 23-45.*

13. Stanley, B.G. and S.F. Leibowitz, *Neuropeptide Y injected in the paraventricular hypothalamus: a powerful stimulant of feeding behavior. Proc Natl Acad Sci U S A, 1985.* **82***(11): p. 3940-3.*

14. Wilson, B.D., M.M. Ollmann, and G.S. Barsh, *The role of agouti-related protein in regulating body weight. Mol Med Today, 1999.* **5***(6): p. 250-6.*

15. Luquet, S., et al., *NPY/AgRP neurons are essential for feeding in adult mice but can be ablated in neonates. Science, 2005.* **310***(5748): p. 683-5.*

16. Gropp, E., et al., *Agouti-related peptide-expressing neurons are mandatory for feeding. Nat Neurosci, 2005.* **8***(10): p. 1289-91.*

17. Fan, W., et al., *Role of melanocortinergic neurons in feeding and the agouti obesity syndrome. Nature, 1997.* **385***(6612): p. 165-8.*

18. Kristensen, P., et al., *Hypothalamic CART is a new anorectic peptide regulated by leptin. Nature, 1998.* **393***(6680): p. 72-6.*

19.   Vong, L., et al., *Leptin action on GABAergic neurons prevents obesity and reduces inhibitory tone to POMC neurons. Neuron, 2011.* **71**(1): p. 142-54.

20.   Smart, J.L. and M.J. Low, *Lack of proopiomelanocortin peptides results in obesity and defective adrenal function but normal melanocyte pigmentation in the murine C57BL/6 genetic background. Ann N Y Acad Sci, 2003.* **994**: p. 202-10.

21.   Huszar, D., et al., *Targeted disruption of the melanocortin-4 receptor results in obesity in mice. Cell, 1997.* **88**(1): p. 131-41.

22.   O'Rahilly, S. and I.S. Farooqi, *The Genetics of Obesity in Humans, in Endotext, L.J. De Groot, et al., Editors. 2000, MDText.com, Inc.: South Dartmouth (MA).*

23.   Larsen, P.J. and R.G. Hunter, *The role of CART in body weight homeostasis. Peptides, 2006.* **27**(8): p. 1981-6.

24.   Rorato, R., et al., *Prostaglandin mediates endotoxaemia-induced hypophagia by activation of pro-opiomelanocortin and corticotrophin-releasing factor neurons in rats. Exp Physiol, 2009.* **94**(3): p. 371-9.

25.   Liu, J., et al., *The melanocortinergic pathway is rapidly recruited by emotional stress and contributes to stress-induced anorexia and anxiety-like behavior. Endocrinology, 2007.* **148**(11): p. 5531-40.

26.   Fink, G., D.W. Pfaff, and J.E. Levine, eds. *Handbook of Neuroendocrinology. 1st ed. 2012, Academic Press: London, UK. 894.*

27.   Fekete, C. and R.M. Lechan, *Central regulation of hypothalamic-pituitary-thyroid axis under physiological and pathophysiological conditions. Endocr Rev, 2014.* **35**(2): p. 159-94.

28.   Geerling, J.C., et al., *Paraventricular hypothalamic nucleus: axonal projections to the brainstem. J Comp Neurol, 2010.* **518**(9): p. 1460-99.

29.   O'Hare, J.D. and A. Zsombok, *Brain-liver connections: role of the preautonomic PVN neurons. Am J Physiol Endocrinol Metab, 2016.* **310**(3): p. E183-9.

30.   Hill, J.W., *PVN pathways controlling energy homeostasis. Indian J Endocrinol Metab, 2012.* **16**(Suppl 3): p. S627-36.

31.   Xiang, H.B., et al., *Central circuits regulating the sympathetic outflow to lumbar muscles in spinally transected mice by retrograde transsynaptic transport. Int J Clin Exp Pathol, 2014.* **7**(6): p. 2987-97.

32.   Currie, P.J. and D.V. Coscina, *Regional hypothalamic differences in neuropeptide Y-induced feeding and energy substrate utilization. Brain Res, 1996.* **737**(1-2): p. 238-42.

33.   Bishop, C., P.J. Currie, and D.V. Coscina, *Effects of three neurochemical stimuli on delayed feeding and energy metabolism. Brain Res, 2000.* **865**(1): p. 139-47.

34.   Kotz, C.M., et al., *Effect of NPY in the hypothalamic paraventricular nucleus on uncoupling proteins 1, 2, and 3 in the rat. Am J Physiol Regul Integr Comp Physiol, 2000.* **278**(2): p. R494-8.

35.   Stanley, B.G., et al., *Repeated hypothalamic stimulation with neuropeptide Y increases daily carbohydrate and fat intake and body weight gain in female rats. Physiol Behav, 1989. **46**(2): p. 173-7.*

36.   Parker, R.M. and H. Herzog, *Regional distribution of Y-receptor subtype mRNAs in rat brain. Eur J Neurosci, 1999. **11**(4): p. 1431-48.*

37.   Holliday, N.D., M.C. Michel, and H.M. Cox, *NPY receptor subtypes and their signal transduction, in Neuropeptide Y and Related Peptides, M.C. Michel, Editor. 2004, Springer: Berlin. p. 45-73.*

38.   Pedragosa-Badia, X., J. Stichel, and A.G. Beck-Sickinger, *Neuropeptide Y receptors: how to get subtype selectivity. Front Endocrinol (Lausanne), 2013. **4**: p. 5.*

39.   Fekete, C., et al., *Neuropeptide Y has a central inhibitory action on the hypothalamic-pituitary-thyroid axis. Endocrinology, 2001. **142**(6): p. 2606-2613.*

40.   Fuzesi, T., et al., *Contribution of noradrenergic and adrenergic cell groups of the brainstem and agouti-related protein-synthesizing neurons of the arcuate nucleus to neuropeptide-y innervation of corticotropin-releasing hormone neurons in hypothalamic paraventricular nucleus of the rat. Endocrinology, 2007. **148**(11): p. 5442-50.*

41.   Harris, M., et al., *Transcriptional regulation of the thyrotropin-releasing hormone gene by leptin and melanocortin signaling. J Clin Invest, 2001. **107**(1): p. 111-20.*

42.   Spengler, D., et al., *Identification and characterization of a 3',5'-cyclic adenosine monophosphate-responsive element in the human corticotropin-releasing hormone gene promoter. Mol Endocrinol, 1992. **6**(11): p. 1931-41.*

43.   Melnick, I., et al., *Developmental switch in neuropeptide Y and melanocortin effects in the paraventricular nucleus of the hypothalamus. Neuron, 2007. **56**(6): p. 1103-15.*

44.   Shrestha, Y.B., K. Wickwire, and S.Q. Giraudo, *Role of AgRP on Ghrelin-induced feeding in the hypothalamic paraventricular nucleus. Regul Pept, 2006. **133**(1-3): p. 68-73.*

45.   Wirth, M.M., et al., *Paraventricular hypothalamic alpha-melanocyte-stimulating hormone and MTII reduce feeding without causing aversive effects. Peptides, 2001. **22**(1): p. 129-34.*

46.   Balthasar, N., et al., *Divergence of melanocortin pathways in the control of food intake and energy expenditure. Cell, 2005. **123**(3): p. 493-505.*

47.   Fekete, C., et al., *alpha-Melanocyte-stimulating hormone is contained in nerve terminals innervating thyrotropin-releasing hormone-synthesizing neurons in the hypothalamic paraventricular nucleus and prevents fasting-induced suppression of prothyrotropin-releasing hormone gene expression. J Neurosci, 2000. **20**(4): p. 1550-8.*

48.   Fekete, C., et al., *alpha-Melanocyte stimulating hormone prevents fasting-induced suppression of corticotropin-releasing hormone gene expression in the rat hypothalamic paraventricular nucleus. Neurosci Lett, 2000. **289**(2): p. 152-6.*

49.   Péterfi, Z., et al., *Endocannabinoid and Nitric Oxide Retrograde Signaling Systems in the Hypothalamic Paraventricular Nucleus Have a Critical Role in Mediating the Effects of Npy on Energy Expenditurein Endocrine Society's 98th Annual Meeting. 2016: Boston, MA.*

50.   Piomelli, D., *The molecular logic of endocannabinoid signalling. Nat Rev Neurosci, 2003.* **4**(*11*): p. 873-84.

51.   Araque, A., et al., *Synaptic functions of endocannabinoid signaling in health and disease. Neuropharmacology, 2017.*

52.   Wittmann, G., et al., *Distribution of type 1 cannabinoid receptor (CB1)-immunoreactive axons in the mouse hypothalamus. J Comp Neurol, 2007.* **503**(*2*): p. 270-9.

53.   Kola, B., et al., *The orexigenic effect of ghrelin is mediated through central activation of the endogenous cannabinoid system. PLoS One, 2008.* **3**(*3*): p. e1797.

54.   Di, S., et al., *Nongenomic glucocorticoid inhibition via endocannabinoid release in the hypothalamus: a fast feedback mechanism. J Neurosci, 2003.* **23**(*12*): p. 4850-7.

55.   Hardingham, N., J. Dachtler, and K. Fox, *The role of nitric oxide in pre-synaptic plasticity and homeostasis. Front Cell Neurosci, 2013.* **7**: p. 190.

56.   Szabadits, E., et al., *Hippocampal GABAergic synapses possess the molecular machinery for retrograde nitric oxide signaling. J Neurosci, 2007.* **27**(*30*): p. 8101-11.

57.   Makara, J.K., et al., *Involvement of nitric oxide in depolarization-induced suppression of inhibition in hippocampal pyramidal cells during activation of cholinergic receptors. J Neurosci, 2007.* **27**(*38*): p. 10211-22.

58.   Affleck, V.S., J.H. Coote, and S. Pyner, *The projection and synaptic organisation of NTS afferent connections with presympathetic neurons, GABA and nNOS neurons in the paraventricular nucleus of the hypothalamus. Neuroscience, 2012.* **219**: p. 48-61.

59.   Gereben, B., et al., *Cellular and molecular basis of deiodinase-regulated thyroid hormone signaling. Endocr Rev, 2008.* **29**(*7*): p. 898-938.

60.   Tu, H.M., et al., *Regional distribution of type 2 thyroxine deiodinase messenger ribonucleic acid in rat hypothalamus and pituitary and its regulation by thyroid hormone. Endocrinology, 1997.* **138**(*8*): p. 3359-68.

61.   Visser, T.J., *Cellular Uptake of Thyroid Hormones, in Endotext, L.J. De Groot, et al., Editors. 2000, MDText.com, Inc.: South Dartmouth (MA).*

62.   Friesema, E.C., et al., *Association between mutations in a thyroid hormone transporter and severe X-linked psychomotor retardation. Lancet, 2004.* **364**(*9443*): p. 1435-7.

63.   Di Cosmo, C., et al., *Mice deficient in MCT8 reveal a mechanism regulating thyroid hormone secretion. J Clin Invest, 2010.* **120**(*9*): p. 3377-88.

64.   Heuer, H., et al., *The monocarboxylate transporter 8 linked to human psychomotor retardation is highly expressed in thyroid hormone-sensitive neuron populations. Endocrinology, 2005.* **146**(*4*): p. 1701-6.

65.   Lechan, R.M. and C. Fekete, *The TRH neuron: a hypothalamic integrator of energy metabolism. Prog Brain Res, 2006.* **153**: p. 209-35.

66.   Lechan, R.M. and I.M. Jackson, *Immunohistochemical localization of thyrotropin-releasing hormone in the rat hypothalamus and pituitary. Endocrinology, 1982.* **111**(*1*): p. 55-65.

67.   Wittmann, G., et al., *Distribution and axonal projections of neurons coexpressing thyrotropin-releasing hormone and urocortin 3 in the rat brain.* J Comp Neurol, 2009. **517**(6): p. 825-40.

68.   Itoh, Y., R. Oishi, and K. Saeki, *Feeding-induced increase in the extracellular concentration of histamine in rat hypothalamus as measured by in vivo microdialysis.* Neuroscience letters, 1991. **125**(2): p. 235-7.

69.   Ookuma, K., et al., *Hypothalamic sites of neuronal histamine action on food intake by rats.* Brain research, 1989. **490**(2): p. 268-75.

70.   Yasuda, T., et al., *Dual regulatory effects of orexins on sympathetic nerve activity innervating brown adipose tissue in rats.* Endocrinology, 2005. **146**(6): p. 2744-8.

71.   Fulop, A.K., et al., *Hyperleptinemia, visceral adiposity, and decreased glucose tolerance in mice with a targeted disruption of the histidine decarboxylase gene.* Endocrinology, 2003. **144**(10): p. 4306-14.

72.   Gotoh, K., et al., *Hypothalamic neuronal histamine mediates the thyrotropin-releasing hormone-induced suppression of food intake.* Journal of neurochemistry, 2007. **103**(3): p. 1102-10.

73.   Parmentier, R., et al., *Excitation of histaminergic tuberomamillary neurons by thyrotropin-releasing hormone.* The Journal of neuroscience : the official journal of the Society for Neuroscience, 2009. **29**(14): p. 4471-83.

74.   Trajkovic, M., et al., *Abnormal thyroid hormone metabolism in mice lacking the monocarboxylate transporter 8.* J Clin Invest, 2007. **117**(3): p. 627-35.

75.   Biag, J., et al., *Cyto- and chemoarchitecture of the hypothalamic paraventricular nucleus in the C57BL/6J male mouse: a study of immunostaining and multiple fluorescent tract tracing.* J Comp Neurol, 2012. **520**(1): p. 6-33.

76.   Corthell, J.T., *Basic Molecular Protocols in Neuroscience: Tips, Tricks, and Pitfalls* 2014: Elsevier Inc.

77.   Deli, L., et al., *Type 1 cannabinoid receptor-containing axons innervate hypophysiotropic thyrotropin-releasing hormone-synthesizing neurons.* Endocrinology, 2009. **150**(1): p. 98-103.

78.   Fekete, C. and Z. Liposits, *Histamine-immunoreactive neurons of the tuberomammillary nucleus are innervated by α-melanocyte stimulating hormone-containing axons. Generation of a new histamine antiserum for ultrastructural studies.* Brain Research, 2003. **969**(1-2): p. 70-77.

79.   Fukudome, Y., et al., *Two distinct classes of muscarinic action on hippocampal inhibitory synapses: M2-mediated direct suppression and M1/M3-mediated indirect suppression through endocannabinoid signalling.* Eur J Neurosci, 2004. **19**(10): p. 2682-92.

80.   Yoshida, T., et al., *Localization of diacylglycerol lipase-alpha around postsynaptic spine suggests close proximity between production site of an endocannabinoid, 2-arachidonoyl-glycerol, and presynaptic cannabinoid CB1 receptor.* J Neurosci, 2006. **26**(18): p. 4740-51.

81.   Narushima, M., et al., *Tonic enhancement of endocannabinoid-mediated retrograde suppression of inhibition by cholinergic interneuron activity in the striatum.* J Neurosci, 2007. **27**(3): p. 496-506.

82. Miura, E., et al., Expression and distribution of JNK/SAPK-associated scaffold protein JSAP1 in developing and adult mouse brain. J Neurochem, 2006. **97**(5): p. 1431-46.

83. Wittmann, G., et al., Efferent projections of thyrotropin-releasing hormone-synthesizing neurons residing in the anterior parvocellular subdivision of the hypothalamic paraventricular nucleus. J Comp Neurol, 2009. **515**(3): p. 313-30.

84. Sarvari, A., et al., Thyrotropin-releasing hormone-containing axons innervate histaminergic neurons in the tuberomammillary nucleus. Brain Res, 2012. **1488**: p. 72-80.

85. Wolf, F.G.a.J.F., Metal-Catalyzed Oxidation Renders Silver Intensification Selective Histochemistry and Cytochemistry, 1986. **34**(12): p. 5.

86. Liposits, Z., G. Setalo, and B. Flerko, Application of the silver-gold intensified 3,3'-diaminobenzidine chromogen to the light and electron microscopic detection of the luteinizing hormone-releasing hormone system of the rat brain. Neuroscience, 1984. **13**(2): p. 513-25.

87. Liposits Z, S.G., Flerkó B., Application of the silver-gold intensified 3,3'-diaminobenzidine chromogen to the light and electron microscopic detection of the luteinizing hormone-releasing hormone system of the rat brain. Neuroscience, 1984. **13**(2): p. 13.

88. Liposits Z1, S.L., Paull WK., Neuropeptide-Y and ACTH-immunoreactive innervation of corticotropin releasing factor (CRF)-synthesizing neurons in the hypothalamus of the rat. An immunocytochemical analysis at the light and electron microscopic levels. Histochemistry 1988. **88**(3-6): p. 7.

89. Harlow E, L.D., Antibodies A laboratory manual. 1988, USA: Cold Spring Harbor Laboratory.

90. Wittmann, G., et al., Medullary adrenergic neurons contribute to the neuropeptide Y-ergic innervation of hypophysiotropic thyrotropin-releasing hormone-synthesizing neurons in the rat. Neurosci Lett, 2002. **324**(1): p. 69-73.

91. Branchereau P, V.B.E., Chan J, Pickel VM., Ultrastructural characterization of neurons recorded intracellularly in vivo and injected with lucifer yellow: advantages of immunogold-silver vs. immunoperoxidase labeling. Microsc Res Tech, 1995. **1;30**(5): p. 11.

92. Dehmelt, L. and S. Halpain, The MAP2/Tau family of microtubule-associated proteins. Genome Biology, 2005. **6**(1): p. 204-204.

93. Kalló, I., et al., A Novel Pathway Regulates Thyroid Hormone Availability in Rat and Human Hypothalamic Neurosecretory Neurons. PLoS ONE, 2012. **7**(6): p. e37860.

94. Fekete, C., et al., Neuropeptide Y1 and Y5 receptors mediate the effects of neuropeptide Y on the hypothalamic-pituitary-thyroid axis. Endocrinology, 2002. **143**(12): p. 4513-9.

95. Fekete C, K.J., Mihály E, Sarkar S, Rand WM, Légrádi G, Emerson CH, Lechan RM., Neuropeptide Y Has a Central Inhibitory Action on the Hypothalamic-Pituitary-Thyroid Axis. Endocrinology, 2001. **142**(6): p. 7.

96. Fekete, C., et al., Agouti-related protein (AGRP) has a central inhibitory action on the hypothalamic-pituitary-thyroid (HPT) axis; comparisons between the effect of AGRP and neuropeptide Y on energy homeostasis and the HPT axis. Endocrinology, 2002. **143**(10): p. 3846-53.

97. Wittmann, G., et al., Origin of cocaine- and amphetamine-regulated transcript-containing axons innervating hypophysiotropic corticotropin-releasing hormone-synthesizing neurons in the rat. Endocrinology, 2005. **146**(7): p. 2985-91.

98. Lechan, R.M. and I.M.D. Jackson, Immunohistochemical Localization of Thyrotropin-Releasing Hormone in the Rat Hypothalamus and Pituitary*. Endocrinology, 1982. **111**(1): p. 55-65.

99. Arch, J.R., et al., Some mathematical and technical issues in the measurement and interpretation of open-circuit indirect calorimetry in small animals. Int J Obes (Lond), 2006. **30**(9): p. 1322-31.

100. Even, P.C., A. Mokhtarian, and A. Pele, Practical aspects of indirect calorimetry in laboratory animals. Neurosci Biobehav Rev, 1994. **18**(3): p. 435-47.

101. Weir, J.B., New methods for calculating metabolic rate with special reference to protein metabolism. J Physiol, 1949. **109**(1-2): p. 1-9.

102. Even, P.C. and N.A. Nadkarni, Indirect calorimetry in laboratory mice and rats: principles, practical considerations, interpretation and perspectives. Am J Physiol Regul Integr Comp Physiol, 2012. **303**(5): p. R459-76.

103. Ruffin, M.P., et al., Metabolic action of neuropeptide Y in relation to its effect on feeding. Physiol Behav, 1997. **62**(6): p. 1259-64.

104. Challet, E., P. Pevet, and A. Malan, Effect of prolonged fasting and subsequent refeeding on free-running rhythms of temperature and locomotor activity in rats. Behav Brain Res, 1997. **84**(1-2): p. 275-84.

105. Opiol, H., et al., Ultrasonic vocalizations in rats anticipating circadian feeding schedules. Behav Brain Res, 2015. **284**: p. 42-50.

106. Xu, B., et al., Daily changes in hypothalamic gene expression of neuropeptide Y, galanin, proopiomelanocortin, and adipocyte leptin gene expression and secretion: effects of food restriction. Endocrinology, 1999. **140**(6): p. 2868-75.

107. Inagaki N, T.K., Taniuchi I, Panula P, Yamatodani A, Tohyama M, Watanabe T, Wada H., An analysis of histaminergic efferents of the tuberomammillary nucleus to the medial preoptic area and inferior colliculus of the rat. Exp Brain Res., 1990. **80**(2): p. 7.

108. Panula P, Y.H., Costa E., Histamine-containing neurons in the rat hypothalamus. Proc Natl Acad Sci U S A, 1984. **81**(8): p. 5.

109. Dube, M.G., et al., Neuropeptide Y release is elevated from the microdissected paraventricular nucleus of food-deprived rats: an in vitro study. Endocrinology, 1992. **131**(2): p. 684-8.

110. Rethelyi, M. and V. Fockter, The fiber architecture of the rat median eminence with some accidental observations on the significance of tanycyte processes. Acta Biol Acad Sci Hung, 1982. **33**(2-3): p. 289-300.

111. Du, J.L., et al., Long-range retrograde spread of LTP and LTD from optic tectum to retina. Proc Natl Acad Sci U S A, 2009. **106**(45): p. 18890-6.

112. Fekete, C. and R.M. Lechan, Negative feedback regulation of hypophysiotropic thyrotropin-releasing hormone (TRH) synthesizing neurons: role of neuronal afferents and type 2 deiodinase. Front Neuroendocrinol, 2007. **28**(2-3): p. 97-114.

113. *Diano, S., et al., Fasting-induced increase in type II iodothyronine deiodinase activity and messenger ribonucleic acid levels is not reversed by thyroxine in the rat hypothalamus. Endocrinology, 1998. **139**(6): p. 2879-84.*

114. *Fekete, C., et al., Lipopolysaccharide induces type 2 iodothyronine deiodinase in the mediobasal hypothalamus: implications for the nonthyroidal illness syndrome. Endocrinology, 2004. **145**(4): p. 1649-55.*

115. *Fekete, C., et al., Bacterial lipopolysaccharide (LPS)-induced type 2 iodothyronine deiodinase (D2) activation in the mediobasal hypothalamus (MBH) is independent of the LPS-induced fall in serum thyroid hormone levels. Brain Res, 2005. **1056**(1): p. 97-9.*

116. *Mohácsik, P., et al. Infection-Induced Increase in Type 2 Deiodinase Expression Is Accompanied By an Increase in Thyroid Hormone Action in the Mediobasal Hypothalamus. in Endocrine Society's 98th Annual Meeting. 2016. Boston, MA.*

117. *Freitas, B.C., et al., Paracrine signaling by glial cell-derived triiodothyronine activates neuronal gene expression in the rodent brain and human cells. J Clin Invest, 2010. **120**(6): p. 2206-17.*

118. *Lechan, R.M. and C. Fekete, Role of thyroid hormone deiodination in the hypothalamus. Thyroid, 2005. **15**(8): p. 883-97.*

119. *Dawson, A., Thyroidectomy progressively renders the reproductive system of starlings (Sturnus vulgaris) unresponsive to changes in daylength. J Endocrinol, 1993. **139**(1): p. 51-5.*

120. *Nakao, N., et al., Thyrotrophin in the pars tuberalis triggers photoperiodic response. Nature, 2008. **452**(7185): p. 317-22.*

121. *Baumgartner, A., et al., Rat brain type II 5'-iodothyronine deiodinase activity is extremely sensitive to stress. J Neurochem, 1998. **71**(2): p. 817-26.*

122. *Araki, O., et al., Expression of type 2 iodothyronine deiodinase in corticotropin-secreting mouse pituitary tumor cells is stimulated by glucocorticoid and corticotropin-releasing hormone. Endocrinology, 2003. **144**(10): p. 4459-65.*

123. *Giustina, A. and W.B. Wehrenberg, Influence of thyroid hormones on the regulation of growth hormone secretion. Eur J Endocrinol, 1995. **133**(6): p. 646-53.*

124. *Nishiwaki-Ohkawa, T. and T. Yoshimura, Molecular basis for regulating seasonal reproduction in vertebrates. J Endocrinol, 2016. **229**(3): p. R117-27.*

125. *Fekete, E.M., et al., Delayed satiety-like actions and altered feeding microstructure by a selective type 2 corticotropin-releasing factor agonist in rats: intra-hypothalamic urocortin 3 administration reduces food intake by prolonging the post-meal interval. Neuropsychopharmacology, 2007. **32**(5): p. 1052-68.*

126. *Ishibashi, H., et al., Excitation of locus coeruleus noradrenergic neurons by thyrotropin-releasing hormone. J Physiol, 2009. **587**(Pt 23): p. 5709-22.*

127. *Zhang, L., M. Kolaj, and L.P. Renaud, GIRK-like and TRPC-like conductances mediate thyrotropin-releasing hormone-induced increases in excitability in thalamic paraventricular nucleus neurons. Neuropharmacology, 2013. **72**: p. 106-15.*

128.   Hara, J., et al., Thyrotropin-releasing hormone increases behavioral arousal through modulation of hypocretin/orexin neurons. J Neurosci, 2009. **29**(12): p. 3705-14.

129.   Ballerini, L., et al., Electrophysiological interactions between 5-hydroxytryptamine and thyrotropin releasing hormone on rat hippocampal CA1 neurons. Eur J Neurosci, 1994. **6**(6): p. 953-60.

130.   Itoh, Y., R. Oishi, and K. Saeki, Feeding-induced increase in the extracellular concentration of histamine in rat hypothalamus as measured by in vivo microdialysis. Neurosci Lett, 1991. **125**(2): p. 235-7.

131.   Ookuma, K., et al., Hypothalamic sites of neuronal histamine action on food intake by rats. Brain Res, 1989. **490**(2): p. 268-75.

132.   Peters A, P.S., deF Webster H., Neurons and their supporting cells. The fine structure of the nervous system. 1991, Oxford: Oxford University Press.

133.   Gotoh, K., et al., Hypothalamic neuronal histamine mediates the thyrotropin-releasing hormone-induced suppression of food intake. J Neurochem, 2007. **103**(3): p. 1102-10.

134.   Parmentier, R., et al., Excitation of histaminergic tuberomamillary neurons by thyrotropin-releasing hormone. J Neurosci, 2009. **29**(14): p. 4471-83.

135.   Engel, S. and M.C. Gershengorn, Thyrotropin-releasing hormone and its receptors--a hypothesis for binding and receptor activation. Pharmacol Ther, 2007. **113**(2): p. 410-9.

136.   Ericson, H., T. Watanabe, and C. Kohler, Morphological analysis of the tuberomammillary nucleus in the rat brain: delineation of subgroups with antibody against L-histidine decarboxylase as a marker. J Comp Neurol, 1987. **263**(1): p. 1-24.

137.   Miklos, I.H. and K.J. Kovacs, Functional heterogeneity of the responses of histaminergic neuron subpopulations to various stress challenges. Eur J Neurosci, 2003. **18**(11): p. 3069-79.

138.   Mahia, J. and A. Puerto, Lesions of tuberomammillary nuclei induce differential polydipsic and hyperphagic effects. Eur J Neurosci, 2006. **23**(5): p. 1321-31.

139.   Vizi, E.S., et al., Non-synaptic receptors and transporters involved in brain functions and targets of drug treatment. Br J Pharmacol, 2010. **160**(4): p. 785-809.

140.   Yamada, M., T. Satoh, and M. Mori, Mice lacking the thyrotropin-releasing hormone gene: what do they tell us? Thyroid, 2003. **13**(12): p. 1111-21.

141.   Haas, H. and P. Panula, The role of histamine and the tuberomamillary nucleus in the nervous system. Nat Rev Neurosci, 2003. **4**(2): p. 121-30.

142.   Nishino, S., et al., Effects of thyrotropin-releasing hormone and its analogs on daytime sleepiness and cataplexy in canine narcolepsy. J Neurosci, 1997. **17**(16): p. 6401-8.

143.   Ko, E.M., et al., Wake-related activity of tuberomammillary neurons in rats. Brain Res, 2003. **992**(2): p. 220-6.